Cancer Biology & Therapy 12:8, 665-679; October 15, 2011; © 2011 Landes Bioscience

Using magnetic resonance imaging and spectroscopy in cancer diagnostics and monitoring

Preclinical and clinical approaches

Risto A. Kauppinen[1] and Andrew C. Peet[2]

[1]Clinical Research and Imaging Centre and Department of Experimental Psychology; University of Bristol; Bristol, UK;
[2]Cancer Sciences; University of Birmingham and Birmingham Children's Hospital NHS Foundation Trust; Birmingham, UK

Keywords: magnetic resonance imaging, magnetic resonance spectroscopy, cancer, metabolism, hypoxia, angiogenesis, imaging biomarkers

Abbreviations: ADC, apparent diffusion coefficient; APTR, amide proton transfer ratio; ASL, arterial spin labeling; BOLD, blood oxygenation level dependent; CP, Carr-Purcell; CNS, central nervous system; CT, computed tomography; DCE, dynamic contrast enhanced; DNP, dynamic nuclear polarization; DSC, dynamic susceptibility contrast; DTI, diffusion tensor imaging; DWI, diffusion weighted imaging; EPR, electron paramagnetic resonance; MR, (nuclear) magnetic resonance; MRI, magnetic resonance imaging; MRS, magnetic resonance spectroscopy; MTR, magnetization transfer ratio; MTT, mean transit time; PET, positron emission tomography; PS, phosphatidyl serine; ptO_2, partial tissue oxygen tension; T_1, longitudinal relaxation time; T_2, transverse relaxation time; T_2*, apparent transverse relaxation time; VASO, vascular space occupancy; VEGF, vascular endothelial growth factor; 3D, three dimensional; 5-FU, 5-fluorouracil

Nuclear Magnetic Resonance (MR) based imaging has become an integrated domain in today's oncology research and clinical management of cancer patients. MR is a unique imaging modality among numerous other imaging modalities by providing access to anatomical, physiological, biochemical and molecular details of tumor with excellent spatial and temporal resolutions. In this review we will cover established and investigational MR imaging (MRI) and MR spectroscopy (MRS) techniques used for cancer imaging and demonstrate wealth of information on tumor biology and clinical applications MR techniques offer for oncology research both in preclinical and clinical settings. Emphasis is given not only to the variety of information which may be obtained but also the complementary nature of the techniques. This ability to determine tumor type, grade, invasiveness, degree of hypoxia, microvacular characteristics and metabolite phenotype, has already profoundly transformed oncology research and patient management. It is evident from the data reviewed that MR techniques will play a key role in uncovering molecular fingerprints of cancer, developing targeted treatment strategies and assessing responsiveness to treatment for personalized patient management, thereby allowing rapid translation of imaging research data into the benefit of clinical oncology.

*Correspondence to: Risto A Kauppinen; Email: psrak@bristol.ac.uk
Submitted: 10/05/10; Revised: 09/02/11; Accepted: 09/18/11
DOI: 10.4161/cbt.12.8.18137

General Introduction to Imaging Techniques

Imaging is an essential component of tumor assessment both in preclinical and clinical settings. Whereas traditionally, it has provided information largely on the tumor size, location and its relationship with adjacent structures, imaging is increasingly providing information on the biological properties of the tumor. This gives an unparalleled opportunity to investigate tumor biology directly in vivo. Since modern therapeutic strategies for cancer management are aimed largely at targeting known biological properties of the tumor, imaging is now providing non-invasive information to guide both drug development and aid therapeutic management in the clinic. This review focuses on MRI and MRS techniques which are routinely used in the clinical environment and also widely used in cancer research. They are able to probe a wide range of tumor properties making them attractive for providing an in vivo biological profile of the tumor. It is important to understand how MRI and MRS fit within the spectrum of imaging modalities which are available for evaluating tumors and these are summarized with respect to their physical properties in **Table 1**.

This review demonstrates the wide range of MR applications available to oncology research and patient management. MR scanners are widely available today and they provide a truly integrated "hybrid" platform for in vivo imaging, i.e., MRI and MRS can be accomplished by the MR equipment with only minor hardware modifications in the same imaging session. MR techniques allow the anatomical, physiological and biochemical data to be acquired non-invasively from virtually any part of the body.

Table 1. Comparison of characteristics for in vivo imaging techniques

Technique	Physics	What is revealed	Resolution (preclinical/clinical)	Duration of scans	Costs
X-RAY/CT (computerised tomography)	X-ray absorption	Organ anatomy, excellent for calcified tissues	Micrometer/ millimeter isotropic	Minutes	Intermediate
ULTRASOUND	Echoes generated to high-frequency sound	Organ anatomy, tissue interfaces, contrast agents for some applications	Micrometer/ millimeter isotropic	Minutes	Low
SPECT (single positron emitting computerised tomography)	Radioactive tracers	Receptor binding, uptake and metabolism of exogenous compounds, heamodynamics	Millimeter/ sub-centimeter in plane (10–20 mm slice)	Tens of minutes	Intermediate
PET (positron emission tomography)	Positron labeled isotope tracers	Receptor binding, gene activity, uptake and metabolism of exogenous compounds, hemodynamics	Submillimeter/ millimeter in plane (5–10 mm slice)	Tens of minutes	High
OPTICAL/NIR (near infrared)	Light scattering/light absorption	Cell surfaces, Hemoglobin, NADH and NADP, cytochromes	Micrometer/ submillimeter (poor depth penetration)	Seconds to minutes	Low
EPR (electron paramagnetic resonance)	Electron paramagnetic resonance, sensing unpaired electrons	Paramagnetic species, partial oxygen pressure (require injection of exogenous reporter)	Millimeter/several millimeter, For oxygenation few hundered micrometer around the probe	Tens of minutes	Intermediate
MRI (magnetic resonance imaging)	Nuclear magnetic resonance, mainly water protons	Anatomy, hemodynamics, edema, vascular properties (use of exogenous contrast agents)	Micrometer/submillimer in plane (0.3–1 mm slice)	Tens of minutes	High
MRS (magnetic resonance spectroscopy)	Nuclear magnetic resonance, exploiting chemical shift of nuclei	Endogenous metabolites, energy state, pH, Mg^{2+} activity Metabolic fluxes using ^{13}C or ^{15}N labeled substrates	Few microliter / 0.5 mL for ^{1}H 100 microliter / 25 mL for ^{31}P	Tens of minutes	High

In addition to the endogenous molecules exploited for imaging exogenous contrast agents are available to bring further biological targets under our scrutiny. The most recent technical developments include targeted-contrast agents[1,2] and dynamic nuclear polarization (DNP) for hyperpolarizing stable isotopes.[3,4] We will review the use of MR techniques in imaging multiple aspects of cancer both in preclinical and clinical settings. Our goal is several-fold: (a) to highlight the wealth of information available from cancer anatomy, physiology and metabolism by multimodal MR (**Fig. 1**) (b) to demonstrate the unprecedented use of MR in cancer management and (c) to project the future of cancer imaging by MR and other non-invasive imaging techniques.

MR of Cancer

It is beyond the scope of this review to explain the physics of MR and technical principles of its descendants, such as MRI and MRS,[5] instead we give a short description of the very basics behind in vivo MR signals. Inherent physical properties of water protons, such as relaxation and Brownian motion, together with chemical interactions of water with macromolecules (chiefly with proteins and polypeptides, but also with lipid-containing species) and exchange between cells and subcellular compartments, provide the basis for MRI in living systems. The MRI signal can also be rendered sensitive to key physiological parameters, such as blood flow. Furthermore, the immediate magnetic environment of water protons strongly influences the signal in specific MRI scans, such as T_2 and T_2* MRI. MRI pulse sequences can be designed to probe selectively many of the chemical and/or physical properties of water, such as relaxation or diffusion, to yield the contrast into MR images.

MRS exploits the property that atomic nuclei in different electric environments resonate at slightly different frequencies. Since the electric environments are dictated by the surrounding chemical structure, the resulting resonant frequencies are a characteristic of the chemical groups and molecules present. Since the intensity of the resonance is dependent on the concentration of the metabolite, MRS can provide concentrations of a number of different metabolites non-invasively in vivo, providing a very powerful tool. There are, however, several challenges to using this technique. The resonant frequencies of the different metabolites are very close together and a homogeneous magnetic field is required to ensure that they can be resolved. Bone and air interfaces are therefore difficult regions to collect high quality data from and whole coverage of a given body part is not usually obtained. Metabolites are present in very small concentrations compared with the amount of water in tissue and so signals are very weak and low spatial resolution is

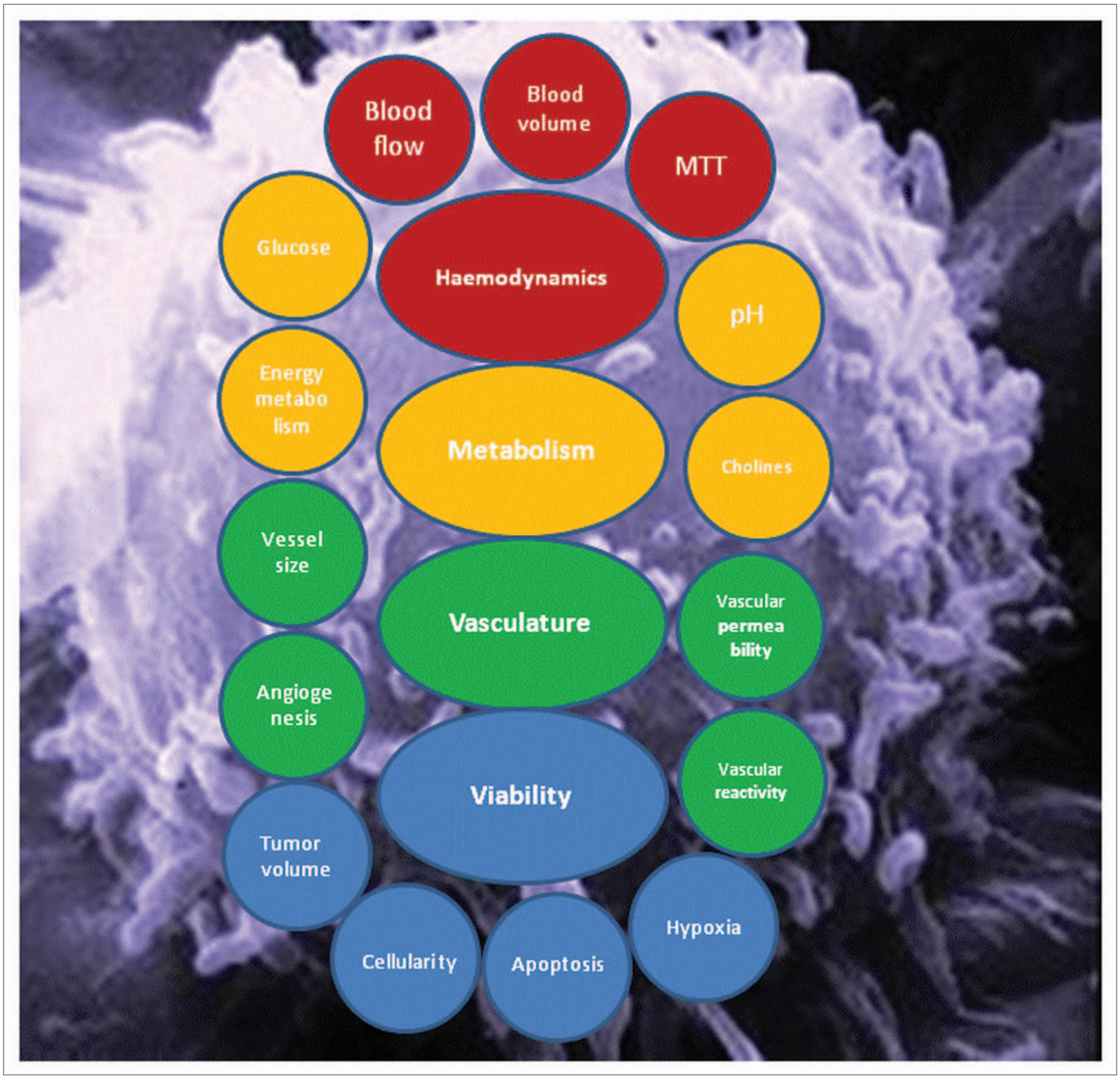

Figure 1. Schematic summary of in vivo properties of tumors that are probed by MR techniques.

obtained clinically, typically in cm^3, and only the metabolites present in millimolar concentrations are detectable.

Since the early applications of MR,[6] it has become apparent that MRI can provide not only exquisite detail on structure but also probe tissue properties. Today's requirements for any imaging modality for oncology applications is toward more specific molecular, biochemical and cellular details from cancer in situ for accurate diagnosis, prognosis and treatment monitoring. The surge of new multimodal MR techniques over the past decade or so has assured a rapid progress and ever increasing number of new applications of MR as illustrated in this review and elsewhere.[7-9] Advanced MR techniques have already made personalized medicine a reality in cancer treatment by revealing responders and non-responders early on before the tumor volume changes enabling clinicians to adjust anticancer therapies accordingly.[8,10] Elusive goals in clinical practice are being achieved, such as determining cancer prognosis from MR scan at the time of primary diagnosis and prior to surgical tissue biopsies. Below we will give details of cancer applications of several MR techniques, yet the list below is not exhaustive and we advise the readers to consult recent literature for further information.

Use of Conventional MRI in Oncology: From Diagnosis and Beyond

The concept of conventional (or standard) MRI has been commonly adopted in the literature embracing longitudinal relaxation (T_1), transverse relaxation (T_2) and proton density images. The underpinning mechanism for image intensity, and consequently, for contrast in conventional MR images is chiefly governed by relaxation processes of water protons as well as the total water content in tissue. For example, free water appears dark in T_1 (see lateral ventricles in **Fig. 2A**) and bright in T_2 (see lateral ventricles in **Fig. 2B**) images, and species with short T1 (such as white matter in brain) are bright in T_1 scans (**Fig. 2A**), whereas species with short T_2 (such as iron-containing basal ganglia) are

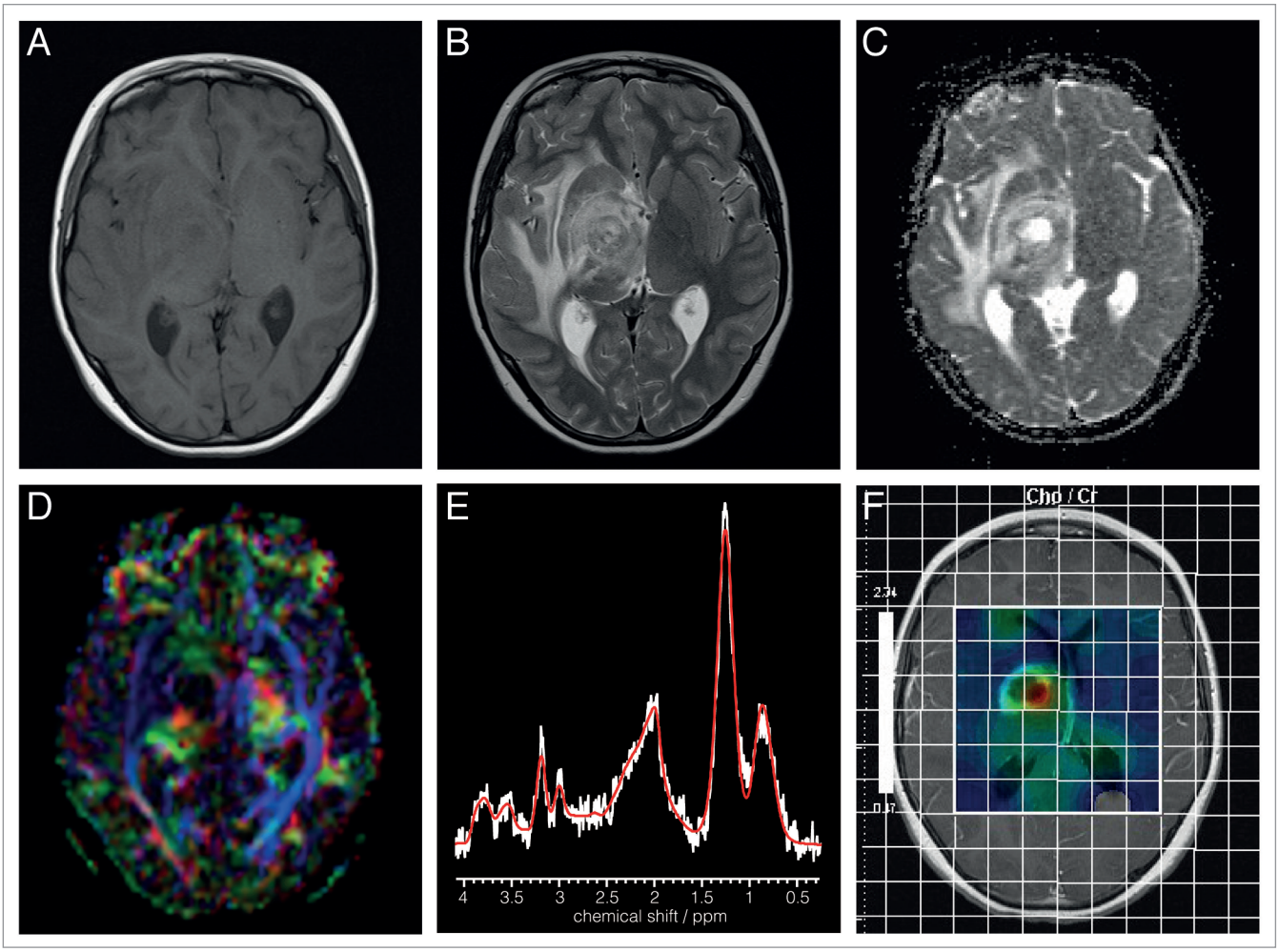

Figure 2. Axial MR images from a patient with a right thalamic high grade glioma acquired at 1.5T (A) T_1-weighted; (B) T_2-weighted; (C) DWI; (D) fractional anisotropy image (E) $_1$H MRS from the tumor core with major peaks assigned as follows: Choline-containing compounds (3.23ppm), total creatine (at 3.03 ppm) and mobile lipids (at 2.0, 1.3 and 0.9 ppm); (F) Choline-containing compounds-to-total creatine (Cho/Cr) ratio image from multivoxel MRS represented as a color map on a T_1-weighted image acquired after injection of a Gd- contrast agent.

dark in T_2 scans (**Fig. 2B**). The proton density image represents water content, as the image is acquired with minimal T_1 and T_2 weighting to eliminate signal losses due to T_1 and T_2 relaxations.

The conventional MRI techniques form the workhorse for tumor assessment in clinical radiology, but also in monitoring tumor volume in preclinical models of cancer. These images are acquired at high anatomical resolution in minutes and these factors make them attractive for tumor volume assessment. The main biological source for MR contrast between healthy tissue and tumor is the water content. An example is shown in **Figure 2** for a brain tumor where tumor itself appear isointense in T_1 (**Fig. 2A**) but bright, with heterogeneous signal, in T_2 images (**Fig. 2B**). Peritumor edema gives a strong signal in T_2 images (**Fig. 2B**) due to high tissue water content and mobility. Similarly, cysts containing pure water-like liquid and hemorrhages within tumors are revealed with high anatomical precision.

It should be stressed that the conventional MRI techniques allow biophysical factors other than water content to be exploited for image contrast. For instance, T_2 images acquired using the so-called Car-Purcell (CP) technique render the image signal sensitive to dynamic properties of water, governed by diffusion and susceptibility dephasing. Using the CP acquisition for T_2 images one can eliminate signal from free water rendering areas of tumor MR visible where water dynamics is changing due to ongoing cell death in response to cytotoxic therapy[11] (**Fig. 3**). A previous study indicates that the bright, the so-called dynamic dephasing signal, appears in responding glioma tissue before tumor shrinks.[11]

Diffusion MR for Cancer Imaging: Improved Treatment Monitoring

Brownian motion of molecules, termed as diffusion, is governed by the thermal motion of molecules. Diffusion of water in vivo can be probed for MRI contrast and since implementation into MRI in 1990[12] this contrast has been demonstrated to possess numerous applications, in particular in monitoring tumor treatment in vivo. Diffusion weighted imaging (DWI) both in preclinical cancer models and cancer patients has demonstrated that the value of

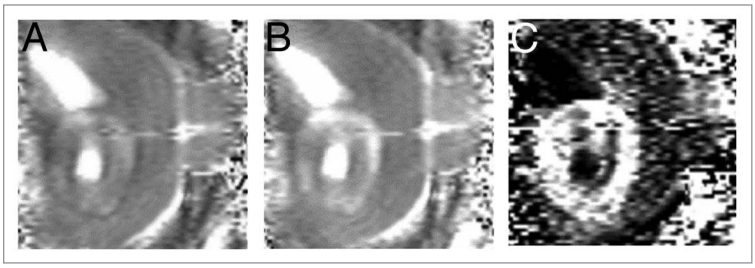

Figure 3. A BT4C rat glioma imaged at 4.7 T using Carr-Purcell (CP) multi-echo MRI. A BT4C glioma bearing rat was treated with herpes simplex virus thymidine kinase-ganciclovir gene therapy. (A) Shows a CP MR image acquired with short and panel (B) with long interpulse interval. Panel (C) is a normalized difference image of images shown in panels (A) and (B) yielding the so-called dynamic dephasing contrast. It should be noted that in this image (C) free water gives no signal and thus both ventricles and a tumor cyst appear dark. Instead, the tumor tissue undergoing cytotoxic cell death shows bright signal that is not obvious from either of the images in (A) and (B). Courtesy of Dr. Olli H.J. Grohn, University of Eastern Finland, Kuopio, Finland.

DWI in cancer monitoring is several-fold.[9,13] This is partially due to the fact that diffusion contrast sensitizes MR images, among others, to tumor cellularity and microenvironment.[13-15]

DWI has demonstrated heterogeneity in the apparent diffusion coefficient (ADC) within solid tumors (for an ADC image, see **Fig. 2C**) in numerous organs. ADC images are generated from two or more sub-images acquired with different diffusion weighting factors. Low ADC in tumor is associated with high cell density,[16,17] fibrosis and other alterations in the tumor microenvironment leading to increased tortuosity in the extracellular space.[18] This is understood by the restrictions imposed by cell structures, high intracellular-to-extracellular volume ratio and elevated macromolecule content in tumor per unit volume.[13] The converse is also true, i.e., lowered cell density results in elevated ADC.[17]

Evidence is also emerging that DWI performed prior to treatment can predict progression of some cancers.[15,18] In prostate cancer, ADC varies according to the location of tumor. In peripheral zone tumors, high ADC is associated with benign tumors, and thus, ADC is able to predict tumor aggressiveness.[19] In locally advanced breast cancer, low tumor ADC was shown to predict good response to neoadjuvant chemotherapy.[20] Using ADC as an imaging biomarker it has been shown that malignant and benign breast tumors can be differentiated with sensitivity and specificity of 89 and 77%, respectively.[21] Similarly, ADC can be used to separate malignant and benign hepatic lesions.[22] In addition, diffusion MRI has shown great potential for separating benign from malignant head and neck tumors and thereby guiding biopsing.[23] Recent technical advancements in body MR have indicated that DWI may provide valuable information for lymph node staging,[24] which has recently been possible in situ only by radionucleotide techniques, such as PET. Affected nodes show ADCs that differ from unaffected nodes. In lymphomatous nodes ADC has been found to be low, whereas metastases in nodes appear to result in high ADC values.[9] Whole body DWI MRI with background suppression has been recently introduced to cancer staging.[25,26] The whole body DWI MRI has been shown to be as accurate as PET with CT (PET/CT) to staging lymphomas[25] and parenchymal neoplasms in the body.[26] It is anticipated that whole body DWI MRI integrated with morphological MRI scans will greatly increase diagnostic accuracy of cancers by MRI.

One of the most promising applications for DWI is monitoring of treatment response to radiation and/or anticancer agents. As mentioned above, ADC is influenced by cell density and consequently, an increase in ADC after anticancer therapy may indicate response before the tumor volume begins to shrink.[17,27] Chenevert et al.[14] introduced the use of histogram analysis of ADC in brain tumors to predict responders. In cases with successful treatment the ADC histogram shifts to the right, in contrast to non-responders where no shift or shift to the left is evident. The approach proved to be more sensitive to detect effective treatment response than either by average tumor ADC or shrinkage of tumor.[14,17] Treated with standard anticancer drugs and/or radiation ADC increases in responding tumors.[15] In contrast, a recent study indicates that ischemia-like decrease in ADC to anti-angiogenic therapy with bevazicumab is detected in brain tumors.[28] Rieger and coworkers observed that decreased ADC was evident in 72% of bevazicumab treated malignant gliomas as early as four weeks after introducing the drug. A biopsy from one low ADC lesion showed atypical necrosis and upregulation of hypoxia-inducible factor 1-α. These data indicate that bevazicumab by blocking neovascularisation may effectively decrease the supply of nutrients and starve the glioblastomas of oxygen and other energy substrates.

A clinically burdening issue concerns distinguishing between recurrence and treatmen-related necrosis in patient follow up. DWI may provide clinically valuable information to address this issue. It has been observed that the magnitude of ADC will be informative, low ADC in treated brain tumor is indicative of a recurrence, whereas elevated ADC reflects edema and/or necrosis due to treatment.[29] The accuracy of ADC to discriminate between tumor recurrence and treatment necrosis is improved by combining it with MRS.[30] However, published reports so far show no fully consistent pattern for ADC in recurrent tumors and more work is required to clarify the position for ADC in detection of tumor recurrence.[31]

A recently developed diffusion MRI technique, diffusion tensor imaging (DTI),[32,33] provides orientation-specific information for water diffusion. DTI is now in common use to track axons and nerve fibers in the brain.[33] Interestingly, recent data show that DTI can help to delineate the influence of tumors on surrounding brain parenchyma and to differentiate tumor from peritumor brain tissue.[34] DTI has been shown to be very useful for planning brain tumor resections by enabling the position of fiber tracts to be visualized with respect to the tumor.[35] **Figure 2D** gives a DTI image from a brain tumor patient. Wang and coworkers reported recently that quantitative diffusion parameters obtained by DTI allow separation of glioblastomas from brain metastates and primary lymphomas.[36]

Incorporation of DWI into oncology MRI protocols has prompted the need for quantitative images rather than observer

interpreted film reading as traditionally performed in Radiology. In addition to quantitative images, forming so called parametric maps, which then can be analyzed using multivariate procedures, such as pattern recognition, principal component analysis, independent component analysis and neural networks.

Magnetization Transfer and Amide Proton Transfer Rate MRI

Magnetization transfer (MT) through either dipolar or non-dipolar mechanisms is a common phenomenon in vivo due to differing molecular mobilities of water protons in different physico-chemical environments.[37] MT MRI contrast has been shown to be beneficial for clinical diagnosis of tumors. In brain tumors MT contrast, more specifically the so-called MT ratio (MTR), is lower than in gray or white matter, a state that is thought to reflect altered water-to-macromolecule ratio in tumor parenchyma.[38,39] Preliminary MTR data indicate that it may be useful also for brain[38] and breast tumor[40] grading. MT has also been introduced to delineate lung tumors for radiotherapy planning.[41]

A special case of MT contrast is the recently introduced amide proton transfer ratio (APTR).[42] APTR probes magnetization exchange between amide protons in macromolecules and bulk water protons and is accomplished by setting the off-resonance saturation on the specific resonance frequency of amide protons.[42] APTR allows the assessment of protein and peptide content of tumors[43] and it gains contributions from pH as well.[42] APTR MRI has been applied to imaging of brain tumors indicating that this new MRI technique may be able to distinguish between tumor recurrence and treatment-related necrosis, an important clinical issue in management of glioma patients.[44]

In the context of MT MRI, it is worth mentioning rotating frame relaxation MRI, the $T_{1\rho}$ MRI.[45] Strictly speaking $T_{1\rho}$ MRI is a form of relaxation governed MR contrasts, however, it is often associated with MT MRI.[46] Using $T_{1\rho}$ and MT MRI in combination it was observed that malignant and benign head and neck tumors can be separated with these MR contrasts with specificity exceeding 90%.[46] Similarly, $T_{1\rho}$ MRI has been shown to possess unprecedented sensitivity to highlight early treatment response in preclinical tumor models.[47] Noninvasive information from tumors in situ afforded by MT-based and $T_{1\rho}$ MR techniques is substantially adding to the overall picture depicted above for conventional and diffusion MRI.

ASL and Blood Volume MRI: Probing Hemodynamics and Vascular Reactivity

MRI offers a truly non-invasive access both into blood flow and blood volume in vivo. An MRI technique called arterial spin labeling (ASL) can be used to image and quantify tissue perfusion (~blood flow).[48,49] ASL MRI is accomplished by applying rf-pulses to the arterial blood proximal (i.e., to the heart side) to the organ under study to magnetically label the water in the blood entering the tissue. The labeled blood exchanges with tissue water at the capillary level, resulting in decrease in (T_1)-MRI signal intensity that is proportional to perfusion.[49] One of the strengths of ASL MRI is that one can obtain absolute blood flow with similar accuracy as with PET, but with better spatial resolution than obtained with PET.

ASL is used chiefly in the assessment of brain and kidney tumors due to favorable hemodynamic properties in these organs for the MRI perfusion technique.[50] ASL of orthotopic animal brain tumor models has shown uniformly low perfusion in tumor stroma compared with brain parenchyma.[51] ASL studies of human brain tumors, however, show heterogeneous perfusion patterns.[52-54] This is not unexpected in the light of known heterogeneity of oxygenation in many brain tumor types. Interestingly, ASL perfusion measurements indicate that astrocytic tumors can be graded as low or high grade tumors by means of quantitative perfusion. Low grade gliomas show lower maximum perfusion than high grade gliomas,[52-54] yet the global perfusion in all glioma classes does not differ.[54] High grade gliomas show higher blood flow than CNS lymphomas.[52] These studies are very promising toward the use of ASL MRI for both presurgical brain tumor grading as well as for monitoring treatment responses, for instance in the case of anti-angiogenic drugs.[50]

Blood volume, the key index of hemodynamics, can be determined by MRI either using exogenous contrast agent (see the section below) or with a blood MR signal nulling technique, the so called VASO MRI (VAscular Space Occupancy).[55] So far, VASO MRI has been used to image blood volume in brain tumors. Lu et al.[56] studied 39 glioma patients with VASO MRI, where the VASO signal was acquired in a manner rendering it sensitive to both blood volume and vascular permeability. Lu et al. reported that low grade gliomas have lower blood volume than high grade ones, the discrimination accuracy of 97% was found. Interestingly, blood volume as determined by VASO MRI showed a tendency the discriminate between low and high grade gliomas. The current VASO MRI protocols allow only for partial coverage of the whole brain, but nevertheless the VASO data, as part of multimodal MR assessment of brain tumors, are promising for presurgical evaluation of brain cancers.

DSC and DCE MRI: Revealing Quantitative Properties of Vasculature

Properties of tumor vasculature, including microperfusion, vascular permeability, vessel density and vessel size, are crucial indices of neovascularisation (or angiogenesis) in cancer tissue.[57] MRI provides a window to image these indices and thus, angiogenesis in cancer in vivo.[58-60] The techniques used to this end require injection of exogenous contrast agents that are commonly used in clinical imaging with MR data acquisition accomplished using fast imaging techniques, such as echo planar imaging (EPI). The two MRI techniques, the so-called dynamic susceptibility contrast (DSC)[61] and dynamic contrast enhanced (DCE)[62] MRI are targeted to quantify properties of microperfusion and vasculature. DSC is commonly accomplished by acquiring MRI signal by an apparent transverse relaxation (T_2*) MRI technique[61] in rapid succession following rapid iv bolus of Gd-based contrast agent. The passage of the bolus leads to a transient decrease in

T_2* signal, leakage of the contrast agent results in persistently lowered signal that may decrease further as a function of time. The hemodynamic parameters derived from DSC MRI include (relative) blood flow, (relative) blood volume and mean transit time.[61]

DCE MRI[62] involves acquisition of MRI signal using a T_1-weigthed MRI acquired either with EPI or rapid gradient echo techniques, passage of Gd-bolus results in a transient signal increase in tissue with mature (healthy) microvasculature, but in tumors with immature and leaky vasculature a persistent signal increase results. From the DCE signal one can derive quantities describing blood-brain-barrier transfer constant, the microvascular permeability (capillary wall permeability-surface area product), size of extravascular-extracellular space, and capillary blood flow.[62] **Figure 4** illustrates a glioblastoma multiforme case imaged with DCE MRI with quantitative maps generated for microvascular and microenvironmental parameters.

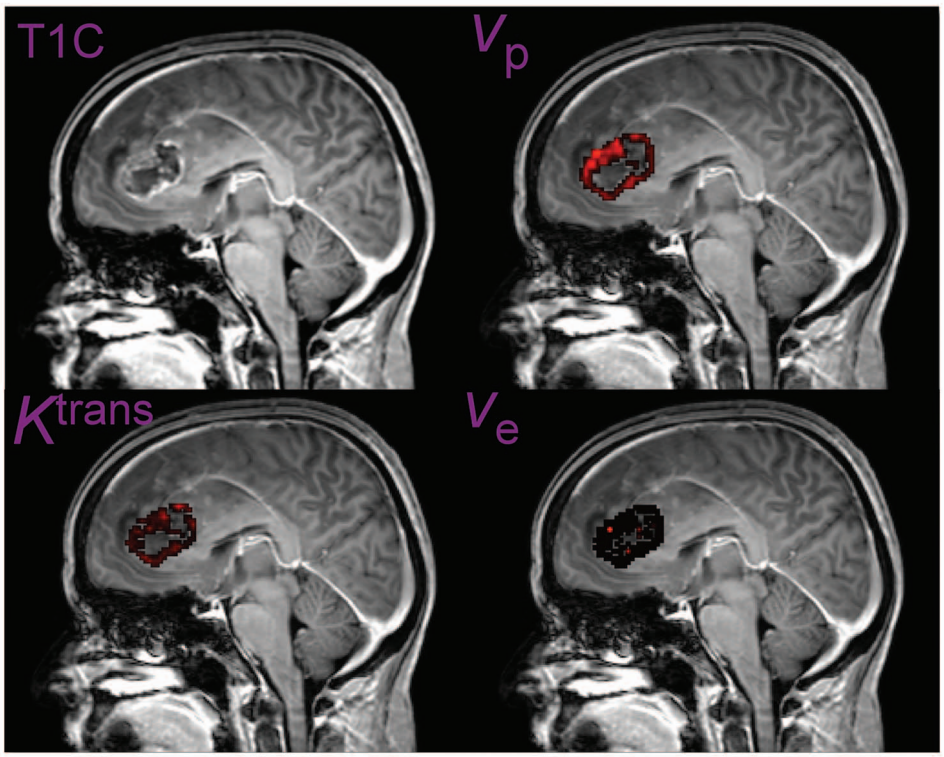

Figure 4. Postcontrast image (T_{1C}), endothelial transfer constant (K_{trans}), extracellular extravascular space (v_e) and blood plasma volume (v_p) maps obtained using DCE MRI in a patient with a glioblastoma multiforme. Courtesy of Drs. Geoffrey Parker and Samantha Mills, University of Manchester, UK.

DSC and DCE MRI have an unprecedented position in evaluation of vascular properties and hemodynamics in tumors in vivo. For instance, in brain lesions the degree of vascular leakiness is an important imaging surrogate in assessment of the nature of the lesion. Malignant lesions show a high degree of leakiness due to rapid angiogenesis with immature microvasculature, whereas benign lesions show vascular leakiness less commonly.[62] Similarly, it is a common observation that cancer recurrence shows a larger degree of leakiness than treatment related necroses, but it should be borne in minds that contrast enhanced MRI and assessment of microvascular properties by MRI alone may not be accurate enough to allow discrimination of recurrence and treatment-related necrosis . Nevertheless, using advanced analytical routines for DSC MRI, Galban et al.[63] reported that relative blood volume was reduced in patients with progressive disease despite radiation and anticancer therapy relative to lesions with successful treatment response.

Owing to the wide availability and sensitivity of DCE and DSC MRI to neovascular pathologies in tumors, these imaging techniques have become work horses for indirect assessment of angiogenesis in many cancer types.[8,60] At the same time DCE and DSC MRI have gained wide use in evaluating response in tumors in situ to anti-vascular agents, involving both anti-vascular endothelial growth factor (VEGF) and vascular disruption agents.[64,65] The strength of MRI techniques lays in the multitude of information obtained from tumors by MRI. Quantitative hemodynamic and/or microvasular data obtained by DCE MRI from breast,[66] renal[67] and head and neck tumors[68] has shown to provide prognostic information prior to therapy. It has been observed that while anti-VEGF treatment decreases vascular permeability and blood volume, indicating normalization of tumor vasculature, edema in and around tumor also decreases.[65] An example of bevazicumab treatment response was given above, suggesting that this anti-angiogenic drug can lead to an ischemia-like state in responding gliomas.[29]

MRI can also be used to estimate vessel size index (VSI, sometimes referred also to as vessel caliber index) using either endogenous[69] or exogenous contrast agents.[70,71] VSI for cancer imaging exploits contrast agent injection to measure the average diameter of microvasculature in vivo. At the same time MRI allows for the estimation of vessel density.[72] For VSI MRI data are collected from tissue following injection of either iron oxide- or Gd-based contrast agents.[71] The former contrast agents have long plasma half lives, but are not yet commonly licensed for clinical indications. Instead, Gd-based contrast agents are in common clinical use and can thus be used for VSI both in clinical and preclinical settings.[73] VSI provides an excellent measurement for microvascular morphology, however, VSI MRI may not give an accurate enough measure for microvascular morphology.[74] Using VSI MRI in a preclinical colorectal cancer model it was shown that anti-VEGF and anti-neurophilin-1 drugs both reduce VSI and vessel density.[72] In a murine glioma model VSI increased, while blood volume and vascular permeability decreased in response to

cediranib treatment,[73] which is a VEGF-inhibitor. Instead, cediranib treatment of human gliomas leads to decrease in VSI (see ref. 73 for references), with reduced blood volume and vascular permeability underscoring the importance of using appropriate references for treatment response evaluation.

DSC and DCE MRI are unparalled tools for imaging tumor vascular characteristics and angiogenesis. They provide a major advance for individualized treatment response monitoring, with numerous key parameters revealed in vivo for diagnosis and treatment response assessment.

Tumor Hypoxia Probed by MRI

MRI and MRS provide indirect ways of assessing tumor oxygenation. Above it was described how ASL, VASO, DSC and DCE allow the derivation of hemodynamic variables. Of course, perfusion of tissue is the key factor supplying oxygen (and other substrates) for cellular metabolism in vivo. Blood oxygenation level dependent (BOLD) MRI contrast[75] is generated by a change in local deoxy-hemoglobin concentration (Hb). The (Hb)/(HbO_2) ratio will reflect the balance of oxygen delivery (~perfusion) and consumption (~mitochondrial respiration)[76,77] Hb is a paramagnetic species causing dephasing of the transverse magnetization. As a result, both T_2* and T_2 in parenchyma shorten in response to increased (Hb)/(HbO_2) ratio, the former being more sensitive than the latter due to inherent physical difference between these MR variables.

BOLD contrast has been examined as a potential means to indirectly evaluate changes in tumor oxygenation in vivo.[78] The BOLD signal gains complex contributions from blood oxygenation and blood volume and their contributions vary as a function of magnetic field strength and image acquisition parameters, such as echo time.[79] These factors together with inherent variation in intratumor T_2*/T_2 signal due to edema and increased water permeability of tumor vasculature have hampered quantification of tumor oxygenation in absolute terms from the BOLD signal.[78] To measure absolute partial pressure of O_2 in tissue (ptO_2) one would need either invasive techniques, MR contrast agents[80] or electron paramagnetic resonance (EPR).[81]

Several studies have been undertaken to evaluate tumor oxygenation with BOLD MRI. These studies have commonly exploited systemic respiratory challenges by allowing the subjects to breathe either pure O_2 or carbogen which is composed of 95–98% O_2 and 2–5% CO_2.[82-84] Inspiring 100% O_2 will maximally saturate HbO_2 and also increase dissolved O_2 in blood plasma. Inspiring carbogen not only maximally saturates HbO_2, but also induces vasodilation and increased blood flow due to effects of CO_2. Owing to noninvasiveness of the BOLD MRI and good tolerance of respiratory challenges used in preclinical settings, substantial efforts have been directed to human applications of these techniques.[85] In addition to these factors the on-going transition from 1.5–3 T for standard human imaging makes the exploitation of BOLD contrast for tumor imaging more attractive.[86] The largest body of BOLD studies in human cancers is in CNS tumors. This is understandable in many regards, as glioblastomas are one of the most hypoxic and at the same time most fatal human cancers and therefore, a commonly available imaging technique for pretreatment assessment of brain tumor hypoxia would be invaluable.[57] Studies[84,86] indicate that gliomas show heterogeneous T_2* signal changes to carbogen challenge. The heterogeneity has been taken to indicate the inherent patchy nature of perfusion and/or vascular reactivity in these tumors; areas showing no response to carbogen are considered to be severely hypoxic. In a study on meningiomas, it was observed that BOLD response to carbogen was seen only in areas with leakage of injected Gd-based contrast agent, demonstrating that BOLD response is an index of vascular reactivity (and thus, perfusion in the tumor stroma).[82] The BOLD MRI data from respiratory challenges are promising pointing to an imminent potential of BOLD MRI in monitoring tumor vasoreactivity and oxygenation in a clinical setting. In animal models drugs have also been used to cause vasodilation, such as nicotinamide.[78] The conclusions from this work is that well perfused and therefore oxygenated tumor regions can be imaged, but any quantitative data for ptO_2, in a similar manner as obtained by EPR, is difficult to obtain.[78]

Recently, a combined MRI/EPR imaging scanner was constructed, making it possible to obtain concurrent MR images and ^{1}H MR spectra from a tumor with quantitative ptO_2 images by EPR.[87] This hybrid imaging scanner was applied to address the interrelationships between tumor perfusion, lactate concentration and oxygenation in a subcutaneous SCC tumor. The data showed surprisingly that substantial hypoxia was present in well perfused parts of the tumor and that high levels of lactate was found in tumor tissue with normal ptO_2. This type of scanner is currently available only for preclinical applications.

^{23}Na MRI in oncology

^{23}Na is a quadrupolar MR nucleus which has been exploited also for in vivo MRI in oncology. In breast tumors, as revealed by contrast enhanced MRI, tissue sodium concentration was found to be elevated by over 60% relative to the glandular tissue when the tumor was malignant.[88] Bartha and associates quantified ^{1}H MRS metabolites and tissue sodium by ^{23}Na MRI in low grade gliomas.[89] They observed that sodium was elevated in gliomas relative to healthy brain parenchyma and that sodium MR data improved delineation of glioma tissue beyond that by MRS. Rat 9L gliomas have been studied by ^{23}Na MRI during nitrosourea treatment.[90] It has been observed that ^{23}Na signal and ADC changes occur in responders well before tumors started to shrink.[90] In summary, ^{23}Na MRI provides complementary information to the ^{1}H MRI and may prove to be useful for multi-nuclear imaging of cancer, but more work is required to consolidate its position in clinics.

Multinuclear MRS for Cancer Imaging: ^{1}H MRS

^{1}H MRS has provided a wealth of information both clinically and in pre-clinical models. While in principle, any atomic nucleus with a magnetic moment can be used for MRS, to date almost all the clinical data has been collected using ^{1}H MRS owing to its

high inherent sensitivity. The most studied anatomical region is the brain, where N-acetyl aspartate, total choline, creatine, *myo*-inositol, lactate, taurine, glutamate+glutamine, lipids and macromolecules resonate, are commonly measured. More sophisticated analysis and increasing field strength can provide information on additional metabolites. High levels of total choline (for Choline-to-creatine ratio map in a brain tumor see **Fig. 2F**) and its ratio to N-acetyl aspartate is a hallmark of most tumors and has been used to distinguish brain tumors from other lesions.[91,92] Due to inherent high glycolytic activity (i.e., the Warburg effect) several tumor types have high lactate concentration independent of the presence of hypoxia,[93] in fact, ^{1}H MRS data from a preclinical glioma points to production of lactate in well oxygenated part of tumor.[94]

^{1}H MRS has also been used to identify the most active regions of large complex tumors thereby aiding tumor biopsy[95,96] and for delineating tumor margins which can extend beyond the enhancing regions seen on conventional MRI.[95] The entire MRS profile has been shown to be a strong characteristic of tumor type and has been studied extensively as an aid to non-invasive diagnosis, the best results coming from the use of pattern recognition[97-100] Large multi-center studies have shown that this can be robust even when evaluated prospectively[101] and clinical decision support systems based on MRS have been developed.[102,103] High total choline and mobile lipids together with low myo-inositol (for an example brain tumor ^{1}H MRS see **Fig. 2E**) have been identified as markers of high grade particularly in gliomas but also in other CNS tumors.[104,105] More detailed analysis of ^{1}H MRS has revealed other important markers of tumor aggressiveness, such as glycine.[106] Differences have also been found in the primary tumors of medulloblastomas with and without metastatic disease at diagnosis.[107] High total choline and lipids have been identified as biomarkers of poor survival in pediatric tumors.[108] Biomarkers of early response to treatment are also important to identify and there is some indication that MRS can provide this under some circumstances,[109] however, the promising results seen in animal and cell line studies have yet to be mirrored in the clinical arena.

Prostate cancer is a disease in which ^{1}H MRS is being used increasingly to identify regions at high risk of being malignant. Identifying these regions on conventional imaging is difficult and multiple biopsies are usually taken. High resolution, 3-dimensional (3D), multivoxel MRS can give good coverage of the prostate, commonly with an endorectal coil but increasingly with coil arrays placed on the abdomen. Choline and creatine may not be resolvable in a conventional clinical scanner, but a high combined total choline+creatine/citrate ratio is a good correlate of malignancy and can be used to identify the best regions to biopsy.[110] In comparison with histopathology, up to 91% specificity and 95% sensitivity was achieved when MRI was combined with 3D MRSI.[111] The Gleeson score obtained from multiple prostate biopsies together with prostate specific antigen levels in the blood are used to determine clinical management such as the prospect of surgical cure[112] and several studies have now shown a correlation between the MRS parameters and Gleeson score.[113,114] Furthermore the magnitude of the change in total choline+creatine/citrate correlates with the how aggressive the tumors are.[115] With this success, attention is increasingly turning to performing clinical trials which can evaluate the use and predictive nature of these biomarkers.[116]

In breast cancer, response of neoadjuvant chemotherapy is an important indicator of survival and MRS has been investigated as a marker of early response.[117-119] Total choline is high in breast cancer and reduces in patients with MRI and histopathological response.[120] Furthermore, a reduction of total choline between pre-treatment and within 24 h of the first chemotherapy dose correlates significantly with changes in tumor size.[121,122]

^{1}H MRS provides direct access to key aspects of tumor hypoxia. Lactate, the end product of anaerobic glycolysis, is ready detected, however, as stated above interpretation of the presence of lactate in tumor is not unproblematic. Lactate is produced by oxygenated tumor cells in vivo[94] and hence, lactate is found by ^{1}H MRS with non-hypoxic ptO_2.[87] Interestingly, ^{1}H MRS detectable lipids[123] may aid in defining hypoxic tumor stroma.[124] ^{1}H MRS detects lipids present in lipid vesicles.[123] In a C6 glioma, displaying strong ^{1}H MRS lipid signals, lipid vesicles were found in histologically verified hypoxic tumor stroma.[124] However, ^{1}H MRS lipids are present in necrotic tumors with no other detectable metabolites[125] and therefore, presence of other metabolites, such as cholines and lactate, may be indicative to hypoxia in viable tumor stroma rather than necrosis.

^{31}P MRS. ^{31}P MRS was used to perform many of the earliest clinical MRS studies,[126] but has become relatively neglected and at present is only used in clinical centers with a specific interest. It has the advantage over ^{1}H MRS that the individual choline metabolites, phosphocholine and glycerophosphocholine, can be separately detected and these are more robust markers of tumor aggressiveness than the total choline. The studies which have been performed have therefore tended to concentrate on MRS as a biomarker of response rather than diagnosis.[127,128] ATP, ADP and inorganic phosphate can also be detected and used to give a non-invasive measurement of pH and this can be a good indicator of tumor activity and response.[7] ^{31}P MRS suffers from poor sensitivity and voxel volumes of around 27 cm^3 in clinical settings are required. Technical advances in this pursuit such as the availability of higher field strength scanners and the development of new coils may lead to further clinical applications.

^{13}C MRS. While MRS is only sensitive enough to identify the metabolites which are present in the highest of concentrations, there has been much interest in imaging molecules which have been injected into the patient. ^{13}C labeled molecules can be detected with MRS and there have been many studies investigating ^{13}C labeled glucose and its metabolites.[129] The method has the advantage over PET that that the parent molecule and its metabolites can be identified separately. A major advance has come in this field with the use of DNP in which the labeled molecules attain a very high magnetic moment in a process where they are cooled near to the absolute zero.[3] This increases the sensitivity of detection by 10,000-fold and allows detection of small amounts of tracer also by a clinical scanner. Impressive experiments using ^{13}C labeled pyruvate in animal systems shows the metabolism and/or exchange to lactate in real time and shows that this is altered in cancer cells.[4] Disordered energy metabolism

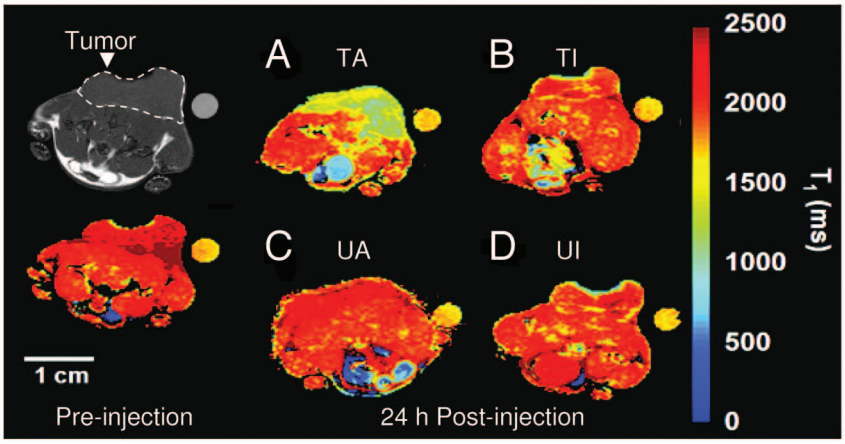

Figure 5. Transverse T_1 maps of drug-treated and untreated EL-4 tumors in animals injected with PS-active (GST-C2A-Gd) and PS-inactive (GST-C2A-Gd) contrast agents. Color scale indicates T_1 values for image voxels. In this example, contrast agents were matched for relaxation rate. Images were acquired immediately before injection of contrast agent (a T_1 map acquired from a tumor before injection is shown on the left-hand side) and at 24 h after injection. Reference capillary was placed adjacent to the tumors, which were implanted on lower areas of backs of animals. Position of the tumor is indicated on the gray-scale image. (A) Etoposide+cyclophoshamide-treated tumor in animal injected with PS-active GST-C2A-Gd (TA). (B) Drug combination-treated tumor in animal injected with PS-inactive GST-C2A-Gd (TI). (C) Untreated tumor in animal injected with PS-active GSTC2A-Gd (UA). (D) Untreated tumor in animal injected with PS-inactive GST-C2A-Gd (UI). Drug combination-treated tumor in an animal injected with PS-active contrast agent shows greater accumulation at 24 h after injection (A). Courtesy of Dr. Kevin Brindle, University of Cambridge, UK.

is a hallmark of cancer cells and this technique offers a direct means of measuring it in vivo. Animal models have also been studied by ^{13}C labeled fumarate which gives specific information on necrosis[130] and ^{13}C labeled bicarbonate which gives information on pH.[131] These techniques have high potential and clinical studies are already underway using ^{13}C labeled pyruvate to investigate prostate cancer.

^{19}F MRS. ^{19}F is an inherently sensitive MR nucleus being only slightly inferior in sensitivity to ^{1}H. ^{19}F concentration in vivo is very low so that there is no background MR signal in vivo. These two factors have been turned to advantage in MR detection of exogenous ^{19}F containing compounds, such as indicators for tissue oxygenation and anticancer drugs. Several ^{19}F tagged compounds have been introduced to quantify ptO_2 as indicated above.[80] ^{19}F MRS has proven to be a unique tool to monitor uptake, metabolism and wash-out of the anticancer drug 5-fluorouracil (5-FU). 5-FU uptake kinetics has been examined by ^{19}F MRS in Lewis lung carcinoma[132] and RIF-1 tumors.[133] It was shown in the RIF-1 tumors that inhalation of 5% CO_2 improved uptake of 5-FU and also treatment response to the drug.[133] 5-FU is converted into cytotoxic metabolites in target tissue, process that can be visualized by ^{19}F MRS.[132] ^{19}F MRS has been used clinically to monitor 5-FU uptake by liver metastases[134] and to guide dose escalation of 5-FU for optimal therapeutic effect.[135] It was observed that increased uptake by liver metastases correlated with clinical response.[134] ^{19}F MR provides access to tissue oxygenation and guides drug assessment, both applications with potential clinical impact.

MRS of cancer specimens in vitro. As well as in vivo imaging of metabolites, MRS can also be used to obtain metabolite profiles of whole tissue, extracts of tissue and body fluids. High resolution magic angle spinning MR provides excellent metabolite identification of tissue samples as small as 5 mg while keeping them intact for further experiments. This has been used to validate in vivo MRS results[136] and obtain a more detailed metabolite profile of tumor tissue in both patients and animals thereby delineating the metabolic pathways in more detail.[137-141] The technique has also been used for investigating intact cells from cell culture experiments. These approaches have established the importance of phosphocholine, glycerophosphocholine, glutamate, glutamine, glycine and lactate individually as biomarkers of tumor response to treatment across a range of tumor cells and treatment approaches.[142-144] However, no single metabolite is a universal marker of tumor response and attention has turned to using combinations of metabolites for which there is emerging evidence that metabolite profiles exist which are specific to certain types of cell stress and cell death.[142] Studies of animal tissue and whole cells have also shown that polyunsaturated fatty acids are an early marker of cell stress and cell death but have proven difficult to image clinically.[145]

Molecular Imaging with MRI in Cancer Imaging

To complement the multitude of information available from endogenous MR contrasts as well as to increase the molecular specificity of MRI signals in vivo, targeted contrast agents tagged with an MRI detectable moiety have been introduced. The targeted contrast agents have greatly increased molecular specificity of biological targets to be imaged by MRI, such as receptors[146] and products of transgenes.[147,148] Most of the contrast agents offer good specificity to the given target by enhancing either T_1 and/or T_2 relaxation. The former agents provide positive contrast in T_1-images, and the latter ones negative contrast in T_2-images.

Since the revelation of transgene expression by targeted MRI contrast agents[147] bespoke contrast agents have been used to reveal several aspects of cancer in vivo. Zhao et al.[149] generated a synaptotagmin I-based contrast reagent to detect externalized phosphatidyl-serine (PS) in apoptotic lymphomas by MRI. The same group has recently modified the reagent to increase its affinity to PS and to give positive MRI contrast with a view to potential clinical application.[150] **Figure 5** illustrates treatment response in a murine EL-4 lymphoma model to etoposide+cyclophosphamide as revealed with a PS-specific MR molecular contrast agent. Strijkers et al. have developed multi-modal contrast agents for direct detection of angiogenesis activity in tumors.[151] Artemov and coworkers imaged HER-2/neu receptors with MRI in a

preclinical breast cancer model.[146] Hyaluronidase activity was detected by MRI in an ovarian tumor model to assess peritumor angiogenic balance.[152] Until today, targeted contrast agents used for molecular imaging by MRI have only been used in preclinical applications, however, the proof of principle studies in preclinical settings have opened avenues for novel targets for MRI in the clinical assessment of cancer patients.

Collective Picture of MR in Monitoring Cancer

Advancement in imaging has fundamentally changed our way of visualizing cancer in vivo. MR techniques have been the key players in this pursuit and there is continuing evolution of new MR techniques and applications. The wealth of information provided by MRI and MRS on tumor biology is having an increasing clinical impact. Today's images from cancer, such as those generated from multi-modal MR scans, are viewed as multi-parametric quantitative maps rather than just individual qualitative films and they are revealing cancer in vivo in a new comprehensive manner. With the shift toward reliance on quantitative parameters, there are very real challenges to clinical application. Studies with impressive results are invariably from a single center with considerable MR research experience and expertise. In order to have a broad clinical impact, the same investigation must provide the same result in any center, irrespective of the level of research expertise. It is emerging that this requires a complex blend of adherence to common acquisition protocols, strict quality control and robust processing and analysis methods. Where these have been achieved, multi-center results have been similar to those from single centers, however, translating this to a non-research clinical environment remains a significant challenge. Achieving this goal, in particular for some of the more innovative techniques, will require a significant level of investment and cooperation from the scanner manufacturers as well as robust evidence from mutlicenter clinical trials. Despite these challenges, compelling evidence is massing that the increasing availability of these imaging modalities is leading to radical changes in the thinking of cancer biology by sampling it directly in vivo.

Acknowledgments

Support from Medical Research Council, the Engineering and Physical Sciences Research Council, the Cancer Imaging Programme funded by Cancer Research UK, EPSRC, MRC and National Institute for Health Research for research in the author's laboratories that is cited in the review is greatly appreciated. Dr. Martin Wilson (University of Birmingham) kindly constructed **Figure 2**.

References

1. Shah K, Jacobs A, Breakefield XO, Weissleder R. Molecular imaging of gene therapy for cancer. Gene Ther 2004; 11:1175-87; PMID:15141158; http://dx.doi.org/10.1038/sj.gt.3302278.
2. Strijkers GJ, Mulder WJ, van Tilborg GA, Nicolay K. MRI contrast agents: current status and future perspectives. Anticancer Agents Med Chem 2007; 7:291-305; PMID:17504156; http://dx.doi.org/10.2174/187152007780618135.
3. Ardenkjaer-Larsen JH, Fridlund B, Gram A, Hansson G, Hansson L, Lerche MH, et al. Increase in signal-to-noise ratio of > 10,000 times in liquid-state NMR. Proc Natl Acad Sci USA 2003; 100:10158-63; PMID:12930897; http://dx.doi.org/10.1073/pnas.1733835100.
4. Day SE, Kettunen MI, Gallagher FA, Hu DE, Lerche M, Wolber J, et al. Detecting tumor response to treatment using hyperpolarized ^{13}C magnetic resonance imaging and spectroscopy. Nat Med 2007; 13:1382-7; PMID:17965722; http://dx.doi.org/10.1038/nm1650.
5. Gadian DG. Nuclear Magnetic Resonance and Its Applications to Living Systems. 1995, Oxford University Press, Oxford, UK.
6. Griffiths JR, Cady EB, Edwards RHT, McCready VR, Wilkie DR, Wiltshaw E. ^{31}P-NMR studies of human tumor in situ. Lancet 1983; i:1435-6; http://dx.doi.org/10.1016/S0140-6736(83)92375-9.
7. Gillies RJ, Morse DL. In vivo magnetic resonance spectroscopy in cancer. Annu Rev Biomed Eng 2005; 7:287-326; PMID:16004573; http://dx.doi.org/10.1146/annurev.bioeng.7.060804.100411.
8. O'Connor JP, Jackson A, Asselin MC, Buckley DL, Parker GJ, Jayson GC. Quantitative imaging biomarkers in the clinical development of targeted therapeutics: current and future perspectives. Lancet Oncol 2008; 9:766-76; PMID:18672212; http://dx.doi.org/10.1016/S1470-2045(08)70196-7.
9. Padhani AR, Liu G, Koh DM, Chenevert TL, Thoeny HC, Takahara T, et al. Diffusion-weighted magnetic resonance imaging as a cancer biomarker: consensus and recommendations. Neoplasia 2009; 11:102-25; PMID:19186405.
10. Batchelor TT, Duda DG, di Tomaso E, Ancukiewicz M, Plotkin SR, Gerstner E, et al. Phase II study of cediranib, an oral pan-vascular endothelial growth factor receptor tyrosine kinase inhibitor, in patients with recurrent glioblastoma. J Clin Oncol 2010; 28:2817-23; PMID:20458050; http://dx.doi.org/10.1200/JCO.2009.26.3988.
11. Gröhn OHJ, Valonen PK, Lehtimaki KK, Vaisanen TH, Kettunen MI, Yla-Herttuala S, et al. Novel magnetic resonance imaging contrast for monitoring response to gene therapy in rat glioma. Cancer Res 2003; 63:7571-4; PMID:14633668.
12. Moseley ME, Cohen Y, Mintorovitch J, Chileuitt L, Shimizu H, Kucharczyk J, et al. Early detection of regional cerebral ischemia in cats: comparison of diffusion- and T2-weighted MRI and spectroscopy. Magn Reson Med 1990; 14:330-46; PMID:2345513; http://dx.doi.org/10.1002/mrm.1910140218.
13. Kauppinen RA. Monitoring cytotoxic tumor treatment response by diffusion magnetic resonance imaging and proton spectroscopy. NMR Biomed 2002; 15:6-17; PMID:11840548; http://dx.doi.org/10.1002/nbm.742.
14. Chenevert TL, Stegman LD, Taylor JM, Robertson PL, Greenberg HS, Rehemtulla A, et al. Diffusion magnetic resonance imaging: an early surrogate marker of therapeutic efficacy in brain tumors. J Natl Cancer Inst 2000; 92:2029-36; PMID:11121466; http://dx.doi.org/10.1093/jnci/92.24.2029.
15. Padhani AR, Koh DM. Diffusion MR imaging for monitoring of treatment response. Magn Reson Imaging Clin N Am 2011; 19:181-209; PMID:21129641; http://dx.doi.org/10.1016/j.mric.2010.10.004.
16. Gupta RK, Sinha U, Cloughesy TF, Alger JR. Inverse correlation between choline magnetic resonance spectroscopy signal intensity and the apparent diffusion coefficient in human glioma. Magn Reson Med 1999; 41:2-7; PMID:10025604; http://dx.doi.org/10.1002/(SICI)1522-2594(199901)41:1<2::AID-MRM2>3.0.CO;2-Y.
17. Valonen PK, Lehtimaki KK, Vaisanen TH, Kettunen MI, Grohn OH, Yla-Herttuala S, et al. Water diffusion in a rat glioma during ganciclovir-thymidine kinase gene therapy-induced programmed cell death in vivo: correlation with cell density. J Magn Reson Imaging 2004; 19:389-96; PMID:15065161; http://dx.doi.org/10.1002/jmri.20026.
18. Gerstner ER, Sorensen AG. Diffusion and diffusion tensor imaging in brain cancer. Semin Radiat Oncol 2011; 21:141-6; PMID:21356481; http://dx.doi.org/10.1016/j.semradonc.2010.10.005.
19. Verma S, Rajesh A, Morales H, Lemen L, Bills G, Delworth M, et al. Assessment of aggressiveness of prostate cancer: correlation of apparent diffusion coefficient with histologic grade after radical prostatectomy. AJR Am J Roentgenol 2011; 196:374-81; PMID:21257890; http://dx.doi.org/10.2214/AJR.10.4441.
20. Li XR, Cheng LQ, Liu M, Zhang YJ, Wang JD, Zhang AL, et al. ADC values can predict treatment response in patients with locally advanced breast cancer undergoing neoadjuvant chemotherapy. Med Oncol 2011; PMID:21286861; http://dx.doi.org/10.1007/s12032-011-9842-y.
21. Tsushima Y, Takahashi-Taketomi A, Endo K. Magnetic resonance (MR) differential diagnosis of breast tumors using apparent diffusion coefficient (ADC) on 1.5-T. J Magn Reson Imaging 2009; 30:249-55; PMID:19629992; http://dx.doi.org/10.1002/jmri.21854.
22. Goshima S, Kanematsu M, Kondo H, Yokoyama R, Kajita K, Tsuge Y, et al. Diffusion-weighted imaging of the liver: optimizing b value for the detection and characterization of benign and malignant hepatic lesions. J Magn Reson Imaging 2008; 28:691-7; PMID:18777553; http://dx.doi.org/10.1002/jmri.21467.
23. Razek AA. Diffusion-weighted magnetic resonance imaging of head and neck. J Comput Assist Tomogr 2010; 34:808-15; PMID:21084893; http://dx.doi.org/10.1097/RCT.0b013e3181f01796.

24. Thoeny HC. Diffusion-weighted MRI in head and neck radiology: applications in oncology. Cancer Imaging 2011; 10:209-14; PMID:21317090; http://dx.doi.org/10.1102/1470-7330.2010.0030.
25. Abdulqadhr G, Molin D, Astrom G, Suurkula M, Johansson L, Hagberg H, et al. Whole-body diffusion-weighted imaging compared with FDG-PET/CT in staging of lymphoma patients. Acta Radiol 2011; 52:173-80; PMID:21498346; http://dx.doi.org/10.1258/ar.2010.100246.
26. Cafagna D, Rubini G, Iuele F, Maggialetti N, Notaristefano A, Pinto D, et al. Whole-body MR-DWIBS vs. [18F]-FDG-PET/CT in the study of malignant tumors: a retrospective study. Radiol Med (Torino) 2011; In press; PMID:21744252; http://dx.doi.org/10.1007/s11547-011-0708-3.
27. Zhao M, Pipe JG, Bonnett J, Evelhoch JL. Early detection of treatment response by diffusion-weighted ^{1}H-NMR spectroscopy in a murine tumor in vivo. Br J Cancer 1996; 73:61-4; PMID:8554985; http://dx.doi.org/10.1038/bjc.1996.11.
28. Rieger J, Bahr O, Muller K, Franz K, Steinbach J, Hattingen E. Bevacizumab-induced diffusion-restricted lesions in malignant glioma patients. J Neurooncol 2010; 99:49-56; PMID:20035366; http://dx.doi.org/10.1007/s11060-009-0098-8.
29. Sundgren PC, Fan X, Weybright P, Welsh RC, Carlos RC, Petrou M, et al. Differentiation of recurrent brain tumor versus radiation injury using diffusion tensor imaging in patients with new contrast-enhancing lesions. Magn Reson Imaging 2006; 24:1131-42; PMID:17071335; http://dx.doi.org/10.1016/j.mri.2006.07.008.
30. Zeng QS, Li CF, Liu H, Zhen JH, Feng DC. Distinction between recurrent glioma and radiation injury using magnetic resonance spectroscopy in combination with diffusion-weighted imaging. Int J Radiat Oncol Biol Phys 2007; 68:151-8; PMID:17289287; http://dx.doi.org/10.1016/j.ijrobp.2006.12.001.
31. Lambregts DM, Maas M, Riedl RG, Bakers FC, Verwoerd JL, Kessels AG, et al. Value of ADC measurements for nodal staging after chemoradiation in locally advanced rectal cancer-a per lesion validation study. Eur Radiol 2011; 21:265-73; PMID:20730540; http://dx.doi.org/10.1007/s00330-010-1937-x.
32. Basser PJ, Mattiello J, Le Bihan D. MR diffusion tensor spectroscopy and imaging. Biophys J 1994; 66:259-67; PMID:8130344; http://dx.doi.org/10.1016/S0006-3495(94)80775-1.
33. Mori S, Crain BJ, Chacko VP, van Zijl PC. Three-dimensional tracking of axonal projections in the brain by magnetic resonance imaging. Ann Neurol 1999; 45:265-9; PMID:9989633; http://dx.doi.org/10.1002/1531-8249(199902)45:2<265::AID-ANA21>3.0.CO;2-3.
34. Kim S, Pickup S, Hsu O, Poptani H. Diffusion tensor MRI in rat models of invasive and well-demarcated brain tumors. NMR Biomed 2008; 21:208-16; PMID:17530617; http://dx.doi.org/10.1002/nbm.1183.
35. Mori S, Frederiksen K, van Zijl PC, Stieltjes B, Kraut MA, Solaiyappan M, et al. Brain white matter anatomy of tumor patients evaluated with diffusion tensor imaging. Ann Neurol 2002; 51:377-80; PMID:11891834; http://dx.doi.org/10.1002/ana.10137.
36. Wang S, Kim S, Chawla S, Wolf RL, Knipp DE, Vossough A, et al. Differentiation between glioblastomas, solitary brain metastases, and primary cerebral lymphomas using diffusion tensor and dynamic susceptibility contrast-enhanced MR imaging. AJNR Am J Neuroradiol 2011; 32:507-14; PMID:21330399; http://dx.doi.org/10.3174/ajnr.A2333.
37. Henkelman RM, Stanisz GJ, Graham SJ. Magnetization transfer in MRI: a review. NMR Biomed 2001; 14:57-64; PMID:11320533; http://dx.doi.org/10.1002/nbm.683.
38. Okumura A, Kuwata K, Takenaka K, Nishimura Y, Shirakami S, Sakai N, et al. Pulsed off-resonance magnetization transfer for brain tumor in patients. Neurol Res 1998; 20:313-9; PMID:9618694.
39. Pui MH. Magnetization transfer analysis of brain tumor, infection, and infarction. J Magn Reson Imaging 2000; 12:395-9; PMID:10992306; http://dx.doi.org/10.1002/1522-2586(200009)12:3<395::AID-JMRI4>3.0.CO;2-L.
40. Bonini RH, Zeotti D, Saraiva LA, Trad CS, Filho JM, Carrara HH, et al. Magnetization transfer ratio as a predictor of malignancy in breast lesions: preliminary results. Magn Reson Med 2008; 59:1030-4; PMID:18429009; http://dx.doi.org/10.1002/mrm.21555.
41. Arnold JF, Kotas M, Pyzalski RW, Pracht ED, Flentje M, Jakob PM. Potential of magnetization transfer MRI for target volume definition in patients with non-small-cell lung cancer. J Magn Reson Imaging 2008; 28:1417-24; PMID:19025950; http://dx.doi.org/10.1002/jmri.21436.
42. Zhou J, Payen JF, Wilson DA, Traystman RJ, van Zijl PC. Using the amide proton signals of intracellular proteins and peptides to detect pH effects in MRI. Nat Med 2003; 9:1085-90; PMID:12872167; http://dx.doi.org/10.1038/nm907.
43. van Zijl PC, Zhou J, Mori N, Payen JF, Wilson D, Mori S. Mechanism of magnetization transfer during on-resonance water saturation. A new approach to detect mobile proteins, peptides, and lipids. Magn Reson Med 2003; 49:440-9; PMID:12594746; http://dx.doi.org/10.1002/mrm.10398.
44. Zhou J, Tryggestad E, Wen Z, Lal B, Zhou T, Grossman R, et al. Differentiation between glioma and radiation necrosis using molecular magnetic resonance imaging of endogenous proteins and peptides. Nat Med 2011; 17:130-4; PMID:21170048; http://dx.doi.org/10.1038/nm.2268.
45. Sepponen RE, Pohjonen JA, Sipponen JT, Tanttu JI. A method for $T_{1\rho}$ imaging. J Comput Assist Tomogr 1985; 9:1007-11; PMID:4056129; http://dx.doi.org/10.1097/00004728-198511000-00002.
46. Markkola AT, Aronen HJ, Paavonen T, Hopsu E, Sipila LM, Tanttu JI, et al. Spin lock and magnetization transfer imaging of head and neck tumors. Radiology 1996; 200:369-75; PMID:8685328.
47. Hakumäki JM, Grohn OH, Tyynela K, Valonen P, Yla-Herttuala S, Kauppinen RA. Early gene therapy-induced apoptotic response in BT4C gliomas by magnetic resonance relaxation contrast T1 in the rotating frame. Cancer Gene Ther 2002; 9:338-45; PMID:11960284; http://dx.doi.org/10.1038/sj.cgt.7700450.
48. Williams DS, Detre JA, Leigh JS, Koretsky AP. Magnetic resonance imaging of perfusion using spin inversion of arterial water. Proc Natl Acad Sci USA 1992; 89:212-6; PMID:1729691; http://dx.doi.org/10.1073/pnas.89.1.212.
49. Golay X, Hendrikse J, Lim TC. Perfusion imaging using arterial spin labeling. Top Magn Reson Imaging 2004; 15:10-27; PMID:15057170; http://dx.doi.org/10.1097/00002142-200402000-00003.
50. Mueller-Lisse UG, Mueller-Lisse UL. Imaging of advanced renal cell carcinoma. World J Urol 2010; 28:253-61; PMID:20458484; http://dx.doi.org/10.1007/s00345-010-0557-z.
51. Moffat BA, Chenevert TL, Hall DE, Rehemtulla A, Ross BD. Continuous arterial spin labeling using a train of adiabatic inversion pulses. J Magn Reson Imaging 2005; 21:290-6; PMID:15723380; http://dx.doi.org/10.1002/jmri.20268.
52. Weber MA, Zoubaa S, Schlieter M, Juttler E, Huttner HB, Geletneky K, et al. Diagnostic performance of spectroscopic and perfusion MRI for distinction of brain tumors. Neurology 2006; 66:1899-906; PMID:16801657; http://dx.doi.org/10.1212/01.wnl.0000219767.49705.9c.
53. Wolf RL, Wang J, Wang S, Melhem ER, O'Rourke DM, Judy KD, et al. Grading of CNS neoplasms using continuous arterial spin labeled perfusion MR imaging at 3 Tesla. J Magn Reson Imaging 2005; 22:475-82; PMID:16161080; http://dx.doi.org/10.1002/jmri.20415.
54. Chawla S, Wang S, Wolf RL, Woo JH, Wang J, O'Rourke DM, et al. Arterial spin-labeling and MR spectroscopy in the differentiation of gliomas. AJNR Am J Neuroradiol 2007; 28:1683-9; PMID:17893221; http://dx.doi.org/10.3174/ajnr.A0673.
55. Lu H, Law M, Johnson G, Ge Y, van Zijl PC, Helpern JA. Novel approach to the measurement of absolute cerebral blood volume using vascular-space-occupancy magnetic resonance imaging. Magn Reson Med 2005; 54:1403-11; PMID:16254955; http://dx.doi.org/10.1002/mrm.20705.
56. Lu H, Pollack E, Young R, Babb JS, Johnson G, Zagzag D, et al. Predicting grade of cerebral glioma using vascular-space occupancy MR imaging. AJNR Am J Neuroradiol 2008; 29:373-8; PMID:17974612; http://dx.doi.org/10.3174/ajnr.A0794.
57. Jain RK, di Tomaso E, Duda DG, Loeffler JS, Sorensen AG, Batchelor TT. Angiogenesis in brain tumors. Nat Rev Neurosci 2007; 8:610-22; PMID:17643088; http://dx.doi.org/10.1038/nrn2175.
58. Miller JC, Pien HH, Sahani D, Sorensen AG, Thrall JH. Imaging angiogenesis: applications and potential for drug development. J Natl Cancer Inst 2005; 97:172-87; PMID:15687360; http://dx.doi.org/10.1093/jnci/dji023.
59. Wong ET, Brem S. Antiangiogenesis treatment for glioblastoma multiforme: challenges and opportunities. J Natl Compr Canc Netw 2008; 6:515-22; PMID:18492463.
60. Zee YK, O'Connor JP, Parker GJ, Jackson A, Clamp AR, Taylor MB, et al. Imaging angiogenesis of genitourinary tumors. Nat Rev Urol 2010; 7:69-82; PMID:20084077; http://dx.doi.org/10.1038/nrurol.2009.262.
61. Kennan RP, Jager HR. T2- and T2*-w DCE-MRI: Blood perfusion and volume estimation using bolus tracking. 2004; 365-412: Quantitative MRI of the Brain. Tofts PB. Chippenham. John Wiley & Sons Ltd.
62. Parker GJM, Padhani AR. T1-w DCE-MRI: T1-weighted Dynamic Contrast-Enhanced MRI. 2004; 341-64: Quantitative MRI of the Brain. Tofts PS. Chippenham. John Wiley & Sons Ltd.
63. Galbán CJ, Chenevert TL, Meyer CR, Tsien C, Lawrence TS, Hamstra DA, et al. The parametric response map is an imaging biomarker for early cancer treatment outcome. Nat Med 2009; 15:572-6; PMID:19377487; http://dx.doi.org/10.1038/nm.1919.
64. Perini R, Choe R, Yodh AG, Sehgal C, Divgi CR, Rosen MA. Non-invasive assessment of tumor neovasculature: techniques and clinical applications. Cancer Metastasis Rev 2008; 27:615-30; PMID:18506398; http://dx.doi.org/10.1007/s10555-008-9147-6.
65. Gerstner ER, Duda DG, di Tomaso E, Ryg PA, Loeffler JS, Sorensen AG, et al. VEGF inhibitors in the treatment of cerebral edema in patients with brain cancer. Nat Rev Clin Oncol 2009; 6:229-36; PMID:19333229; http://dx.doi.org/10.1038/nrclinonc.2009.14.

66. Pickles MD, Manton DJ, Lowry M, Turnbull LW. Prognostic value of pre-treatment DCE-MRI parameters in predicting disease free and overall survival for breast cancer patients undergoing neoadjuvant chemotherapy. Eur J Radiol 2009; 71:498-505; PMID:18572340; http://dx.doi.org/10.1016/j.ejrad.2008.05.007.
67. Flaherty KT, Rosen MA, Heitjan DF, Gallagher ML, Schwartz B, Schnall MD, et al. Pilot study of DCE-MRI to predict progression-free survival with sorafenib therapy in renal cell carcinoma. Cancer Biol Ther 2008; 7:496-501; PMID:18219225; http://dx.doi.org/10.4161/cbt.7.4.5624.
68. Shukla-Dave A, Lee NY, Jansen JF, Thaler HT, Stambuk HE, Fury MG, et al. Dynamic contrast-enhanced magnetic resonance imaging as a predictor of outcome in head and neck squamous cell carcinoma patients with nodal metastases. Int J Radiat Oncol Biol Phys 2011; In press; PMID:21601373; http://dx.doi.org/10.1016/j.ijrobp.2011.03.006.
69. Shen Y, Ahearn T, Clemence M, Schwarzbauer C. Magnetic resonance imaging of the mean venous vessel size in the human brain using transient hyperoxia. Neuroimage 2011; 55:1063-7; PMID:21224003; http://dx.doi.org/10.1016/j.neuroimage.2010.12.084.
70. Dennie J, Mandeville JB, Boxerman JL, Packard SD, Rosen BR, Weisskoff RM. NMR imaging of changes in vascular morphology due to tumor angiogenesis. Magn Reson Med 1998; 40:793-9; PMID:9840821; http://dx.doi.org/10.1002/mrm.1910400602.
71. Troprès I, Grimault S, Vaeth A, Grillon E, Julien C, Payen JF, et al. Vessel size imaging. Magn Reson Med 2001; 45:397-408; PMID:11241696; http://dx.doi.org/10.1002/1522-2594(200103)45:3<397::AID-MRM1052>3.0.CO;2-3.
72. Ungersma SE, Pacheco G, Ho C, Yee SF, Ross J, van Bruggen N, et al. Vessel imaging with viable tumor analysis for quantification of tumor angiogenesis. Magn Reson Med 2010; 63:1637-47; PMID:20512867; http://dx.doi.org/10.1002/mrm.22442.
73. Farrar CT, Kamoun WS, Ley CD, Kim YR, Catana C, Kwon SJ, et al. Sensitivity of MRI Tumor Biomarkers to VEGFR Inhibitor Therapy in an Orthotopic Mouse Glioma Model. PLoS ONE 2011; 6:e17228; PMID:21390238; http://dx.doi.org/10.1371/journal.pone.0017228.
74. Douma K, Oostendorp M, Slaaf DW, Post MJ, Backes WH, van Zandvoort MA. Evaluation of magnetic resonance vessel size imaging by two-photon laser scanning microscopy. Magn Reson Med 2010; 63:930-9; PMID:20373394; http://dx.doi.org/10.1002/mrm.22248.
75. Ogawa S, Lee TM, Kay AR, Tank DW. Brain magnetic resonance imaging with contrast dependent on blood oxygenation. Proc Natl Acad Sci USA 1990; 87:9868-72; PMID:2124706; http://dx.doi.org/10.1073/pnas.87.24.9868.
76. Buxton RB, Frank LR. A model for the coupling between cerebral blood flow and oxygen metabolism during neural stimulation. J Cereb Blood Flow Metab 1997; 17:64-72; PMID:8978388; http://dx.doi.org/10.1097/00004647-199701000-00009.
77. van Zijl PC, Eleff SM, Ulatowski JA, Oja JM, Ulug AM, Traystman RJ, et al. Quantitative assessment of blood flow, blood volume and blood oxygenation effects in functional magnetic resonance imaging. Nat Med 1998; 4:159-67; PMID:9461188; http://dx.doi.org/10.1038/nm0298-159.
78. Howe FA, Robinson SP, McIntyre DJ, Stubbs M, Griffiths JR. Issues in flow and oxygenation dependent contrast (FLOOD) imaging of tumors. NMR Biomed 2001; 14:497-506; PMID:11746943; http://dx.doi.org/10.1002/nbm.716.
79. Silvennoinen MJ, Clingman CS, Golay X, Kauppinen RA, van Zijl PCM. Comparision of the dependence of blood R2 and R2* on oxygen saturation at 1.5 and 4.7 tesla. Magn Reson Med 2003; 49:47-60; PMID:12509819; http://dx.doi.org/10.1002/mrm.10355.
80. Ruiz-Cabello J, Barnett BP, Bottomley PA, Bulte JW. Fluorine (^{19}F) MRS and MRI in biomedicine. NMR Biomed 2011; 24:114-29; PMID:20842758; http://dx.doi.org/10.1002/nbm.1570.
81. Liu KJ, Bacic G, Hoopes PJ, Jiang JJ, Du HK, Ou LC, et al. Assessment of cerebral pO_2 by EPR oximetry in rodents: effects of anesthesia, ischemia, and breathing gas. Brain Res 1995; 685:91-8; PMID:7583257; http://dx.doi.org/10.1016/0006-8993(95)00413-K.
82. Rijpkema M, Schuuring J, Bernsen PL, Bernsen HJ, Kaanders JH, van der Kogel AJ, et al. BOLD MRI response to hypercapnic hyperoxia in patients with meningiomas: correlation with Gadolinium-DTPA uptake rate. Magn Reson Imaging 2004; 22:761-7; PMID:15234444; http://dx.doi.org/10.1016/j.mri.2004.01.055.
83. Remmele S, Dahnke H, Flacke S, Soehle M, Wenningmann I, Kovacs A, et al. Quantification of the magnetic resonance signal response to dynamic CO2-enhanced imaging in the brain at 3 T: R2* BOLD vs. balanced SSFP. J Magn Reson Imaging 2010; 31:1300-10; PMID:20512881; http://dx.doi.org/10.1002/jmri.22171.
84. Rauscher A, Sedlacik J, Fitzek C, Walter B, Hochstetter A, Kalff R, et al. High resolution susceptibility weighted MR-imaging of brain tumors during the application of a gaseous agent. Rofo 2005; 177:1065-9; PMID:16021537.
85. Yetkin FZ, Mendelsohn D. Hypoxia imaging in brain tumors. Neuroimaging Clin N Am 2002; 12:537-52; PMID:12687910; http://dx.doi.org/10.1016/S1052-5149(02)00029-1.
86. Müller A, Remmele S, Wenningmann I, Clusmann H, Traber F, Flacke S, et al. Intracranial tumor response to respiratory challenges at 3.0 T: impact of different methods to quantify changes in the MR relaxation rate R2*. J Magn Reson Imaging 2010; 32:17-23; PMID:20578006; http://dx.doi.org/10.1002/jmri.22205.
87. Matsumoto S, Hyodo F, Subramanian S, Devasahayam N, Munasinghe J, Hyodo E, et al. Low-field paramagnetic resonance imaging of tumor oxygenation and glycolytic activity in mice. J Clin Invest 2008; 118:1965-73; PMID:18431513.
88. Ouwerkerk R, Jacobs MA, Macura KJ, Wolff AC, Stearns V, Mezban SD, et al. Elevated tissue sodium concentration in malignant breast lesions detected with non-invasive ^{23}Na MRI. Breast Cancer Res Treat 2007; 106:151-60; PMID:17260093; http://dx.doi.org/10.1007/s10549-006-9485-4.
89. Bartha R, Megyesi JF, Watling CJ. Low-grade glioma: correlation of short echo time ^{1}H-MR spectroscopy with ^{23}Na MR imaging. AJNR Am J Neuroradiol 2008; 29:464-70; PMID:18238848; http://dx.doi.org/10.3174/ajnr.A0854.
90. Schepkin VD, Ross BD, Chenevert TL, Rehemtulla A, Sharma S, Kumar M, et al. Sodium magnetic resonance imaging of chemotherapeutic response in a rat glioma. Magn Reson Med 2005; 53:85-92; PMID:15690506; http://dx.doi.org/10.1002/mrm.20332.
91. Möller-Hartmann W, Herminghaus S, Krings T, Marquardt G, Lanfermann H, Pilatus U, et al. Clinical application of proton magnetic resonance spectroscopy in the diagnosis of intracranial mass lesions. Neuroradiology 2002; 44:371-81; PMID:12012120; http://dx.doi.org/10.1007/s00234-001-0760-0.
92. Hourani R, Horska A, Albayram S, Brant LJ, Melhem E, Cohen KJ, et al. Proton magnetic resonance spectroscopic imaging to differentiate between nonneoplastic lesions and brain tumors in children. J Magn Reson Imaging 2006; 23:99-107; PMID:16374884; http://dx.doi.org/10.1002/jmri.20480.
93. Miles KA, Williams RE. Warburg revisited: imaging tumor blood flow and metabolism. Cancer Imaging 2008; 8:81-6; PMID:18390391; http://dx.doi.org/10.1102/1470-7330.2008.0011.
94. García-Martin ML, Herigault G, Remy C, Farion R, Ballesteros P, Coles JA, et al. Mapping extracellular pH in rat brain gliomas in vivo by ^{1}H magnetic resonance spectroscopic imaging: comparison with maps of metabolites. Cancer Res 2001; 61:6524-31; PMID:11522650.
95. Burtscher IM, Skagerberg G, Geijer B, Englund E, Stahlberg F, Holtas S. Proton MR spectroscopy and preoperative diagnostic accuracy: an evaluation of intracranial mass lesions characterized by stereotactic biopsy findings. AJNR Am J Neuroradiol 2000; 21:84-93; PMID:10669230.
96. Preul MC, Caramanos Z, Leblanc R, Villemure JG, Arnold DL. Using pattern analysis of in vivo proton MRSI data to improve the diagnosis and surgical management of patients with brain tumors. NMR Biomed 1998; 11:192-200; PMID:9719573; http://dx.doi.org/10.1002/(SICI)1099-1492(199806/08)11:4/5<192::AID-NBM535>3.0.CO;2-3.
97. Preul MC, Caramanos Z, Collins DL, Villemure JG, Leblanc R, Olivier A, et al. Accurate, noninvasive diagnosis of human brain tumors by using proton magnetic resonance spectroscopy. Nat Med 1996; 2:323-5; PMID:8612232; http://dx.doi.org/10.1038/nm0396-323.
98. Tate AR, Majos C, Moreno A, Howe FA, Griffiths JR, Arus C. Automated classification of short echo time in in vivo ^{1}H brain tumor spectra: a multicenter study. Magn Reson Med 2003; 49:29-36; PMID:12509817; http://dx.doi.org/10.1002/mrm.10315.
99. Panigrahy A, Krieger MD, Gonzalez-Gomez I, Liu X, McComb JG, Finlay JL, et al. Quantitative short echo time ^{1}H-MR spectroscopy of untreated pediatric brain tumors: preoperative diagnosis and characterization. AJNR Am J Neuroradiol 2006; 27:560-72; PMID:16551993.
100. Davies NP, Wilson M, Harris LM, Natarajan K, Lateef S, Macpherson L, et al. Identification and characterisation of childhood cerebellar tumors by in vivo proton MRS. NMR Biomed 2008; 21:908-18; PMID:18613254; http://dx.doi.org/10.1002/nbm.1283.
101. García-Gómez JM, Luts J, Julia-Sape M, Krooshof P, Tortajada S, Robledo JV, et al. Multiproject-multicenter evaluation of automatic brain tumor classification by magnetic resonance spectroscopy. MAGMA 2009; 22:5-18; PMID:18989714; http://dx.doi.org/10.1007/s10334-008-0146-y.
102. Tate AR, Underwood J, Acosta DM, Julia-Sape M, Majos C, Moreno-Torres A, et al. Development of a decision support system for diagnosis and grading of brain tumors using in vivo magnetic resonance single voxel spectra. NMR Biomed 2006; 19:411-34; PMID:16763971; http://dx.doi.org/10.1002/nbm.1016.
103. Celda B, Monleon D, Martinez-Bisbal MC, Esteve V, Martinez-Granados B, Pinero E, et al. MRS as endogenous molecular imaging for brain and prostate tumors: FP6 project "eTUMOR". Adv Exp Med Biol 2006; 587:285-302; PMID:17163172; http://dx.doi.org/10.1007/978-1-4020-5133-3_22.
104. Castillo M, Smith JK, Kwock L. Correlation of myo-inositol levels and grading of cerebral astrocytomas. AJNR Am J Neuroradiol 2000; 21:1645-9; PMID:11039343.
105. Shimizu H, Kumabe T, Shirane R, Yoshimoto T. Correlation between choline level measured by proton MR spectroscopy and Ki-67 labeling index in gliomas. AJNR Am J Neuroradiol 2000; 21:659-65; PMID:10782774.
106. Davies NP, Wilson M, Natarajan K, Sun L, MacPherson L, Brundler MA, et al. Non-invasive detection of glycine as a biomarker of malignancy in childhood brain tumors using in-vivo ^{1}H MRS at 1.5 Tesla confirmed by ex-vivo high-resolution magic-angle spinning NMR. NMR Biomed 2010; 23:80-7; PMID:19795380; http://dx.doi.org/10.1002/nbm.1432.

107. Peet AC, Davies NP, Ridley L, Brundler MA, Kombogiorgas D, Lateef S, et al. Magnetic resonance spectroscopy suggests key differences in the metastatic behaviour of medulloblastoma. Eur J Cancer 2007; 43:1037-44; PMID:17349783; http://dx.doi.org/10.1016/j.ejca.2007.01.019.
108. Marcus KJ, Astrakas LG, Zurakowski D, Zarifi MK, Mintzopoulos D, Poussaint TY, et al. Predicting survival of children with CNS tumors using proton magnetic resonance spectroscopic imaging biomarkers. Int J Oncol 2007; 30:651-7; PMID:17273766.
109. Harris LM, Davies NP, Macpherson L, Lateef S, Natarajan K, Brundler MA, et al. Magnetic resonance spectroscopy in the assessment of pilocytic astrocytomas. Eur J Cancer 2008; 44:2640-7; PMID:18835152; http://dx.doi.org/10.1016/j.ejca.2008.08.012.
110. Kurhanewicz J, Swanson MG, Nelson SJ, Vigneron DB. Combined magnetic resonance imaging and spectroscopic imaging approach to molecular imaging of prostate cancer. J Magn Reson Imaging 2002; 16:451-63; PMID:12353259; http://dx.doi.org/10.1002/jmri.10172.
111. Scheidler J, Hricak H, Vigneron DB, Yu KK, Sokolov DL, Huang LR, et al. Prostate cancer: localization with three-dimensional proton MR spectroscopic imaging–clinicopathologic study. Radiology 1999; 213:473-80; PMID:10551229.
112. Cookson MS, Fleshner NE, Soloway SM, Fair WR. Correlation between Gleason score of needle biopsy and radical prostatectomy specimen: accuracy and clinical implications. J Urol 1997; 157:559-62; PMID:8996356; http://dx.doi.org/10.1016/S0022-5347(01)65201-7.
113. Swindle P, McCredie S, Russell P, Himmelreich U, Khadra M, Lean C, et al. Pathologic characterization of human prostate tissue with proton MR spectroscopy. Radiology 2003; 228:144-51; PMID:12832578; http://dx.doi.org/10.1148/radiol.2281011808.
114. Swanson MG, Vigneron DB, Tabatabai ZL, Males RG, Schmitt L, Carroll PR, et al. Proton HR-MAS spectroscopy and quantitative pathologic analysis of MRI/3D-MRSI-targeted postsurgical prostate tissues. Magn Reson Med 2003; 50:944-54; PMID:14587005; http://dx.doi.org/10.1002/mrm.10614.
115. Swanson MG, Vigneron DB, Tran TK, Sailasuta N, Hurd RE, Kurhanewicz J. Single-voxel oversampled J-resolved spectroscopy of in vivo human prostate tissue. Magn Reson Med 2001; 45:973-80; PMID:11378874; http://dx.doi.org/10.1002/mrm.1130.
116. Crehange G, Maingon P, Gauthier M, Parfait S, Cochet A, Mirjolet C, et al. Early Choline Levels from 3-Tesla MR Spectroscopy After Exclusive Radiation Therapy in Patients with Clinically Localized Prostate Cancer are Predictive of Plasmatic Levels of PSA at 1 Year. Int J Radiat Oncol Biol Phys 2011; In press; PMID:21605949; http://dx.doi.org/10.1016/j.ijrobp.2011.03.008.
117. Mountford CE, Somorjai RL, Malycha P, Gluch L, Lean C, Russell P, et al. Diagnosis and prognosis of breast cancer by magnetic resonance spectroscopy of fine-needle aspirates analysed using a statistical classification strategy. Br J Surg 2001; 88:1234-40; PMID:11531873; http://dx.doi.org/10.1046/j.0007-1323.2001.01864.x.
118. Kvistad KA, Bakken IJ, Gribbestad IS, Ehrnholm B, Lundgren S, Fjosne HE, et al. Characterization of neoplastic and normal human breast tissues with in vivo ^{1}H MR spectroscopy. J Magn Reson Imaging 1999; 10:159-64; PMID:10441019; http://dx.doi.org/10.1002/(SICI)1522-2586(199908)10:2<159::AID-JMRI8>3.0.CO;2-0.
119. Huang W, Fisher PR, Dulaimy K, Tudorica LA, O'Hea B, Button TM. Detection of breast malignancy: diagnostic MR protocol for improved specificity. Radiology 2004; 232:585-91; PMID:15205478; http://dx.doi.org/10.1148/radiol.2322030547.
120. Scholl SM, Pierga JY, Asselain B, Beuzeboc P, Dorval T, Garcia-Giralt E, et al. Breast tumor response to primary chemotherapy predicts local and distant control as well as survival. Eur J Cancer 1995; 31A:1969-75; PMID:8562150; http://dx.doi.org/10.1016/0959-8049(95)00454-8.
121. Jagannathan NR, Kumar M, Seenu V, Coshic O, Dwivedi SN, Julka PK, et al. Evaluation of total choline from in-vivo volume localized proton MR spectroscopy and its response to neoadjuvant chemotherapy in locally advanced breast cancer. Br J Cancer 2001; 84:1016-22; PMID:11308247; http://dx.doi.org/10.1054/bjoc.2000.1711.
122. Meisamy S, Bolan PJ, Baker EH, Gulbache E, Everson LI, Nelson MT, et al. Neoadjuvant chemotherapy of locally advanced breast cancer: predicting response with in vivo ^{1}H MR spectroscopy: a pilot study at 4 T. Radiology 2004; 233:424-31; PMID:15516615; http://dx.doi.org/10.1148/radiol.2332031285.
123. Hakumäki JM, Kauppinen RA. ^{1}H NMR visible lipids in the life and death of cells. Trends Biochem Sci 2000; 25:357-62; PMID:10916153; http://dx.doi.org/10.1016/S0968-0004(00)01614-5.
124. Zoula S, Rijken PF, Peters JP, Farion R, Van der Sanden BP, Van der Kogel AJ, et al. Pimonidazole binding in C6 rat brain glioma: relation with lipid droplet detection. Br J Cancer 2003; 88:1439-44; PMID:12778075; http://dx.doi.org/10.1038/sj.bjc.6600837.
125. Kuesel AC, Donnelly SM, Halliday W, Sutherland GR, Smith ICP. Mobile lipids and metabolic heterogeneity of brain tumors as detectable by ex vivo ^{1}H MR spectroscopy. NMR Biomed 1994; 7:172-80; PMID:7946995; http://dx.doi.org/10.1002/nbm.1940070404.
126. Maris JM, Evans AE, McLaughlin AC, D'Angio GJ, Bolinger L, Manos H, et al. ^{31}P nuclear magnetic resonance spectroscopic investigation of human neuroblastoma in situ. N Engl J Med 1985; 312:1500-5; PMID:3990750; http://dx.doi.org/10.1056/NEJM198506063122307.
127. Koutcher JA, Ballon D, Graham M, Healey JH, Casper ES, Heelan R, et al. ^{31}P NMR spectra of extremity sarcomas: diversity of metabolic profiles and changes in response to chemotherapy. Magn Reson Med 1990; 16:19-34; PMID:2175008; http://dx.doi.org/10.1002/mrm.1910160104.
128. Möller HE, Vermathen P, Rummeny E, Wortler K, Wuisman P, Rossner A, et al. In vivo ^{31}P NMR spectroscopy of human musculoskeletal tumors as a measure of response to chemotherapy. NMR Biomed 1996; 9:347-58; PMID:9176889; http://dx.doi.org/10.1002/(SICI)1099-1492(199612)9:8<347::AID-NBM431>3.0.CO;2-3.
129. Shulman RG, Brown TR, Ugurbil K, Ogawa S, Cohen SM, den Hollander JA. Cellular applications of ^{31}P and ^{13}C nuclear magnetic resonance. Science 1979; 205:160-6; PMID:36664; http://dx.doi.org/10.1126/science.36664.
130. Witney TH, Kettunen MI, Hu DE, Gallagher FA, Bohndiek SE, Napolitano R, et al. Detecting treatment response in a model of human breast adenocarcinoma using hyperpolarised [1-^{13}C]pyruvate and [1,4-^{13}C2]fumarate. Br J Cancer 2010; 103:1400-6; PMID:20924379; http://dx.doi.org/10.1038/sj.bjc.6605945.
131. Gallagher FA, Kettunen MI, Day SE, Hu DE, Ardenkjaer-Larsen JH, Zandt R, et al. Magnetic resonance imaging of pH in vivo using hyperpolarized ^{13}C-labelled bicarbonate. Nature 2008; 453:940-3; PMID:18509335; http://dx.doi.org/10.1038/nature07017.
132. Stevens AN, Morris PG, Iles RA, Sheldon PW, Griffiths JR. 5-fluorouracil metabolism monitored in vivo by ^{19}F NMR. Br J Cancer 1984; 50:113-7; PMID:6743508; http://dx.doi.org/10.1038/bjc.1984.146.
133. McSheehy PM, Robinson SP, Ojugo AS, Aboagye EO, Cannell MB, Leach MO, et al. Carbogen breathing increases 5-fluorouracil uptake and cytotoxicity in hypoxic murine RIF-1 tumors: a magnetic resonance study in vivo. Cancer Res 1998; 58:1185-94; PMID:9515804.
134. Kamm YJ, Heerschap A, van den Bergh EJ, Wagener DJ. ^{19}F-magnetic resonance spectroscopy in patients with liver metastases of colorectal cancer treated with 5-fluorouracil. Anticancer Drugs 2004; 15:229-33; PMID:15014355; http://dx.doi.org/10.1097/00001813-200403000-00006.
135. Schlemmer HP, Bachert P, Semmler W, Hohenberger P, Schlag P, Lorenz WJ, et al. Drug monitoring of 5-fluorouracil: in vivo ^{19}F NMR study during 5-FU chemotherapy in patients with metastases of colorectal adenocarcinoma. Magn Reson Imaging 1994; 12:497-511; PMID:8007780; http://dx.doi.org/10.1016/0730-725X(94)92544-5.
136. Wilson M, Davies NP, Grundy RG, Peet AC. A quantitative comparison of metabolite signals as detected by in vivo MRS with ex vivo ^{1}H HR-MAS for childhood brain tumors. NMR Biomed 2009; 22:213-9; PMID:19067434; http://dx.doi.org/10.1002/nbm.1306.
137. Wilson M, Davies NP, Brundler MA, McConville C, Grundy RG, Peet AC. High resolution magic angle spinning ^{1}H NMR of childhood brain and nervous system tumors. Mol Cancer 2009; 8:6; PMID:19208232; http://dx.doi.org/10.1186/1476-4598-8-6.
138. Griffin JL, Blenkiron C, Valonen PK, Caldas C, Kauppinen RAA. HRMAS ^{1}H NMR spectroscopy and reverse transcription-PCR analysis of apoptosis in a rat glioma. Anal Chem 2006; 78:1546-52; PMID:16503606; http://dx.doi.org/10.1021/ac051418o.
139. Lehtimäki KK, Valonen PK, Griffin JL, Vaisanen TH, Grohn OH, Kettunen MI, et al. Metabolite changes in BT4C rat gliomas undergoing ganciclovir-thymidine kinase gene therapy-induced programmed cell death as studied by ^{1}H NMR spectroscopy in vivo, ex vivo, and in vitro. J Biol Chem 2003; 278:45915-23; PMID:12954643; http://dx.doi.org/10.1074/jbc.M306209200.
140. Hekmatyar SK, Wilson M, Jerome N, Salek RS, Griffin JL, Peet A, et al. Metabolic characterization of cerebellum inthe SMO mice, a model for medulloblastoma, using ^{1}H nuclear magnetic resonance spectroscopy. Br J Cancer 2010; 103:1297-304; PMID:20842126; http://dx.doi.org/10.1038/sj.bjc.6605890.
141. Yang Y, Li C, Nie X, Feng X, Chen W, Yue Y, et al. Metabonomic studies of human hepatocellular carcinoma using high-resolution magic-angle spinning ^{1}H NMR spectroscopy in conjunction with multivariate data analysis. J Proteome Res 2007; 6:2605-14; PMID:17564425; http://dx.doi.org/10.1021/pr070063h.
142. Mirbahai L, Wilson M, Shaw CS, McConville C, Malcomson RD, Griffin JL, et al. ^{1}H magnetic resonance spectroscopy metabolites as biomarkers for cell cycle arrest and cell death in rat glioma cells. Int J Biochem Cell Biol 2011; 43:990-1001; PMID:20633697; http://dx.doi.org/10.1016/j.biocel.2010.07.002.
143. Williams SN, Anthony ML, Brindle KM. Induction of apoptosis in two mammalian cell lines results in increased levels of fructose-1,6-bisphosphate and CDP-choline as determined by ^{31}P MRS. Magn Reson Med 1998; 40:411-20; PMID:9727944; http://dx.doi.org/10.1002/mrm.1910400311.
144. Lutz NW, Tome ME, Cozzone PJ. Early changes in glucose and phospholipid metabolism following apoptosis induction by IFN-gamma/TNF-alpha in HT-29 cells. FEBS Lett 2003; 544:123-8; PMID:12782301; http://dx.doi.org/10.1016/S0014-5793(03)00489-7.

145. Hakumäki JM, Poptani H, Sandmair A-M, Ylä-Herttuala S, Kauppinen RA. ^{1}H MRS detects polyunsaturated fatty acid accumulation during gene therapy of glioma: implications for the in vivo detection of apoptosis. Nat Med 1999; 5:1323-7; PMID:10546002; http://dx.doi.org/10.1038/15279.
146. Artemov D, Mori N, Okollie B, Bhujwalla ZM. MR molecular imaging of the Her-2/neu receptor in breast cancer cells using targeted iron oxide nanoparticles. Magn Reson Med 2003; 49:403-8; PMID:12594741; http://dx.doi.org/10.1002/mrm.10406.
147. Weissleder R, Moore A, Mahmood U, Bhorade R, Benveniste H, Chiocca EA, et al. In vivo magnetic resonance imaging of transgene expression. Nat Med 2000; 6:351-5; PMID:10700241; http://dx.doi.org/10.1038/73219.
148. Cohen B, Ziv K, Plaks V, Israely T, Kalchenko V, Harmelin A, et al. MRI detection of transcriptional regulation of gene expression in transgenic mice. Nat Med 2007; 13:498-503; PMID:17351627; http://dx.doi.org/10.1038/nm1497.
149. Zhao M, Bearegard DA, Loizou L, Davletov B, Brindle KM. Non-invasive detection of apoptosis using magnetic resonance imaging and a targeted contrast agent. Nat Med 2001; 7:1241-4; PMID:11689890; http://dx.doi.org/10.1038/nm1101-1241.
150. Krishnan AS, Neves AA, de Backer MM, Hu DE, Davletov B, Kettunen MI, et al. Detection of cell death in tumors by using MR imaging and a gadolinium-based targeted contrast agent. Radiology 2008; 246:854-62; PMID:18187402; http://dx.doi.org/10.1148/radiol.2463070471.
151. Strijkers GJ, Kluza E, Van Tilborg GA, van der Schaft DW, Griffioen AW, Mulder WJ, et al. Paramagnetic and fluorescent liposomes for target-specific imaging and therapy of tumor angiogenesis. Angiogenesis 2010; 13:161-73; PMID:20390447; http://dx.doi.org/10.1007/s10456-010-9165-1.
152. Shiftan L, Israely T, Cohen M, Frydman V, Dafni H, Stern R, et al. Magnetic resonance imaging visualization of hyaluronidase in ovarian carcinoma. Cancer Res 2005; 65:10316-23; PMID:16288020; http://dx.doi.org/10.1158/0008-5472.CAN-04-3947.